ORNL/TM-6670

Mass Transfer in Two-Phase Nondispersing Liquid-Liquid Contactors with a High-Density-Difference System

C. H. Brown, Jr.

OAK RIDGE NATIONAL LABORATORY
OPERATED BY UNION CARBIDE CORPORATION · FOR THE DEPARTMENT OF ENERGY

DISTRIBUTION OF THIS DOCUMENT IS UNLIMITED

DISCLAIMER

Printed in the United States of America. Available from
National Technical Information Service
U.S. Department of Commerce
5285 Port Royal Road, Springfield, Virginia 22161
Price: Printed Copy $6.50; Microfiche $3.00

ORNL/TM-6670

Contract No. W-7405-eng-26

CHEMICAL TECHNOLOGY DIVISION

MASS TRANSFER IN TWO-PHASE NONDISPERSING LIQUID-LIQUID CONTACTORS WITH A HIGH-DENSITY-DIFFERENCE SYSTEM

C. H. Brown, Jr.

This report was prepared as a thesis and submitted to the Faculty of the Graduate School of The University of Tennessee in partial fulfillment of the degree of Master of Science in the Department of Chemical, Metallurgical, and Polymer Engineering.

Date Published-April 1979

OAK RIDGE NATIONAL LABORATORY
Oak Ridge, Tennessee 37830
operated by
UNION CARBIDE CORPORATION
for the
DEPARTMENT OF ENERGY

THIS PAGE

WAS INTENTIONALLY

LEFT BLANK

ACKNOWLEDGMENTS

The writer wishes to thank Dr. J. S. Watson and Dr. J. R. Hightower, Jr., for their many helpful suggestions during both the experimental and data analysis phases of this project.

A group of students from the M.I.T. School of Chemical Engineering Practice, led by J. Herranz, were instrumental in acquiring a portion of the experimental data. Appreciation is also expressed to James D. Hewitt for his diligent and tireless services in operating the equipment and logging much of the data.

Special thanks are due Martha G. Stewart, Connie L. Begovich, Pamela G. Valliant, Janice T. Shannon, and Debbie S. Brown. Ms. Stewart edited the final manuscript. Ms. Begovich provided essential assistance in computer programming for both regression analysis and preparation of most of the figures. Ms. Valliant, Ms. Shannon, and Ms. Brown typed the final and rough drafts.

Dr. C. D. Scott was instrumental in "gently" prodding the writer to finish this thesis.

A final thanks is due my wife, Donna, and my parents, whose support throughout my academic career has been unbounded.

This research was sponsored by the U. S. Department of Energy under contract W-7405-eng-26 with the Union Carbide Corporation.

THIS PAGE

WAS INTENTIONALLY

LEFT BLANK

ABSTRACT

Mass transfer rates of an electrolyte through a turbulent aqueous film in an agitated two-phase nondispersing liquid-liquid contactor were measured using an aqueous electrolyte solution as the light phase and mercury as the heavy phase. The mass transfer data were correlated by the equation

$$N_{Sh} = \left[0.029 \exp(3.3 \times 10^{-6} N_{Re_M})\right] N_{Re_W}^{0.81} N_{Sc_W}^{0.52} .$$

The mass transfer rates were measured polarographically via the diffusion-limited, electrically driven reduction of quinone at the mercury surface in the contactor. Variables tested were the agitation rate, agitator diameter, phase volume, cell size, and various physical properties (principally viscosity) of the aqueous phase.

The parameters found to be most significant to the mass transfer rate were agitator speed, agitator diameter, and aqueous-phase viscosity. A correlation found in the literature is similar to the correlation developed here, but a new form of the intercept term was developed which correlates mass transfer data over a much wider range of Sherwood numbers than that found in the literature.

THIS PAGE

WAS INTENTIONALLY

LEFT BLANK

TABLE OF CONTENTS

LIST OF TABLES

THIS PAGE

WAS INTENTIONALLY

LEFT BLANK

LIST OF FIGURES

FIGURE PAGE

THIS PAGE

WAS INTENTIONALLY

LEFT BLANK

LIST OF SYMBOLS

A	Interfacial area, m^2
B	Number of Faradays per mole of electrode reaction
C	Concentration, kg-mole/m^3
$C_{(8)}$	Constant in Equation (8)
$\mathscr{D}$	Diffusion coefficient, m^2/sec
F	Faraday constant, coul/kg-mole
I	Electric current, A
J	Molar flow rate, kg-mole/sec
K	Overall mass transfer coefficient, m/sec
M	Mercury flow rate, mg/sec
N	Impeller speed, rps
N_{Re}	Reynolds number, Nd^2/ν, dimensionless
N_{Sc}	Schmidt number, $\nu/\mathscr{D}$, dimensionless
N_{Sh}	Sherwood number, $kd/\mathscr{D}$, dimensionless
N_{We}	Modified Weber number, $Nd(\rho d/\sigma_{equiv})^{0.5}$, dimensionless
Q	Molar flux, kg-mole/m^2-sec
R	Gas constant, joules/kg-mole-K
T	Absolute temperature, K
Z	Valence change, equiv/kg-mole
d	Impeller diameter, m
g	Gravitational constant, m/sec^2
k	Film mass transfer coefficient, m/sec
$\overline{k}$	Average film mass transfer coefficient, m/sec
ℓ	Eddy length, m
m	Henry's law constant, dimensionless

n	Number of data points
p	Number of estimators
t	Drop time, sec
x	Independent variable
y	Dependent variable
α	Constant in Equations (6) and (7)
Φ	Electric potential, v
ν	Kinematic viscosity, m^2/sec
η	Dynamic viscosity, kg/m-sec
Γ	Complete gamma function
τ	Total area, m^2
ρ	Density, kg/m^3
σ	Surface tension, kg/sec^2
σ_{equiv}	Equivalent interfacial tension, $\sigma_i + \ell^2\lvert\Delta\rho\rvert$ g/16
Ψ	Phase interaction factor
ω_∞	Rotational rate of the core liquid, rad/sec
κ_g	Constant in Equation (9)
∇	Gradient

Subscripts

B	Bulk phase
i	Interfacial
1	Light phase
2	Heavy phase
C	Core region
a	Annular region
equiv	Equivalent
$\circ$	Averaged over lifetime of drop

CHAPTER I

INTRODUCTION

Operation with a nondispersing device to prevent contamination of one phase with the other is desirable in some chemical processes that require two-phase contacting; on the other hand, there is also the need for increased mass transfer rates afforded by energy input to the system via agitation. An example of a system using this type of device is the extraction of rare-earth fluorides from the fluoride fuel carrier salt to an intermediate bismuth stream in Molten-Salt Breeder Reactor fuel processing (1). Another potential application of the two-phase nondispersing contactor is in the extraction of tritium from the lithium blanket material of a controlled thermonuclear reactor (2). It has been shown that tritium dissolved in molten lithium is preferentially distributed in the salt phase when the tritium-laden lithium is contacted with a molten salt such as LiCl-KCl eutectic (3). A stirred two-phase contactor could be used in this initial extraction step as well as in the following step where the tritium must be stripped from the eutectic salt phase. There are also other potential large-scale applications of such systems in the processing of molten scrap metal to recover valuable components (4).

Mass transfer data have been reported for the two-phase nondispersing contactor by several researchers. Most of the previous studies, however, have been made with systems in which the physical properties of the two phases are very similar (i.e., an aqueous phase and an organic phase). The potential applications mentioned above would involve fluids with a large density difference. As a prerequisite for reliable design of

contactors with fluid properties which are quite different from those studied previously, it is necessary to have data describing mass transfer characteristics of high-density-difference systems such as the salt-metal systems.

To obtain such data efficiently, it was desirable to model the salt-metal systems by performing an experiment that was relatively inexpensive and permitted rapid data acquisition. This study used the water-mercury system, which has a density ratio, ρ_2/ρ_1, of 13, where ρ_2 and ρ_1 represent the heavy- and light-phase densities, respectively. This density ratio is closer to that of the salt-metal systems, where ρ_2/ρ_1 ranges from about 3 to 8, than is the density ratio of aqueous-organic systems, where $\rho_2/\rho_1 = 1.25$.

A conceptual drawing of a typical nondispersing contactor is given in Figure 1. The two phases are pumped in a countercurrent fashion into and out of the vessel shown. Transfer of species from one phase to the other takes place at the liquid-liquid interface and is promoted by agitation of the two phases via turbines which are positioned in each fluid. Agitation is kept below the point at which one phase is physically dispersed into the adjacent phase.

It was of interest to determine the effects of agitator diameter, phase volume, and cell size on the mass transfer characteristics of the cell, since these parameters are important for scale-up purposes and have not been varied sufficiently in previous studies.

Using an aqueous electrolyte as the light phase and mercury as the heavy phase, electrolyte film mass transfer coefficients were measured polarographically in three contactor cells of square cross section, each

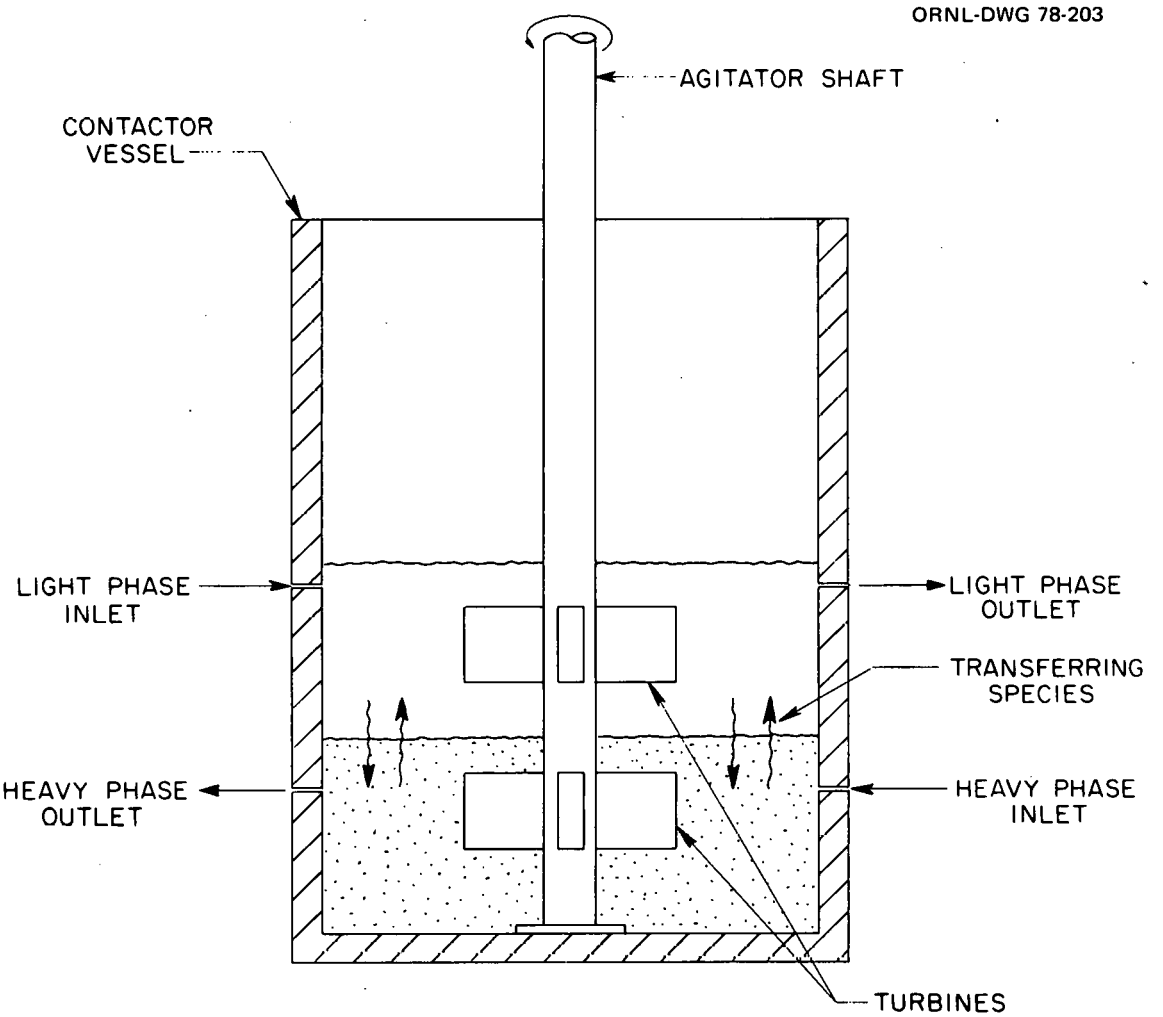

Figure 1. Typical Nondispersing Contactor.

with a different base dimension. The mass transfer coefficient in each cell was measured as a function of agitator rotational speed, agitator diameter, and phase volume. The physical properties of the aqueous phase, principally the viscosity, were varied by the addition of sucrose to the aqueous phase.

The diffusion coefficient of quinone was measured as a function of aqueous-phase viscosity using a dropping mercury electrode (d.m.e.) apparatus. The measured mass transfer rate and the diffusion coefficient data were then utilized to develop a correlation which relates the light-(aqueous-) phase mass transfer coefficient to the significant parameters that were varied in the study.

CHAPTER II

REVIEW OF LITERATURE

Several studies have addressed the problem of mass transport between two agitated, nondispersed liquids. In all cases, however, the research was concentrated on systems where there is only a small density difference between the phases (i.e., aqueous and organic). Most investigators also used cylindrical cells and agitators of approximately the same size. No attempt was made to scale the results obtained in small laboratory-size contactors to larger cells of potential industrial importance.

In general, mass transfer rates have been determined in transient experiments involving mutual solution of one phase into the other. The transient data were obtained in those experiments by sampling each of the phases during an experiment and relying on wet chemical or other secondary techniques for sample analysis.

Lewis (5) used cylindrical, nondispersed, two-phase, mechanically agitated cells to investigate mass transfer rates for several aqueous-organic systems. He correlated his results by the empirical relation

$$\frac{60\ k_1}{\nu_1} = 6.76 \times 10^{-6} \left(N_{Re_1} + N_{Re_2} \frac{\eta_2}{\eta_1} \right)^{1.65} + 1 \ . \qquad (1)$$

Lewis postulated that the mass transfer rate was only a function of eddy transport to and from the interface and was independent of the molecular diffusivity of the observed systems over the range of Reynolds numbers considered. The range of liquid densities covered in his study varied from 0.8 to 1.2 g/cm^3 (800 to 1200 kg/m^3).

Gordon and Sherwood (6) investigated the validity of the additivity of resistances for interphase transfer of solute between two liquids using the mutual saturation technique and various aqueous-organic pairs. The study was essentially an investigation of the validity of using the equation

$$\frac{1}{K_1} = \frac{1}{k_1} + \frac{1}{m\,k_2} \quad , \tag{2}$$

where the first term represents the overall resistance to mass transfer between the two phases, and the second and third terms represent the individual resistances in the stagnant films on either side of the interface. They found good agreement between their data and Equation (2). They also observed that the addition of a surface-active agent to the liquid-liquid interface had little, if any, effect on the mass transfer rate. The results obtained in their study led them to conclude that the individual mass transfer coefficients depend on the molecular diffusivity raised to the one-half power.

McManamey (7) correlated both his data and Lewis' data by the expression

$$\frac{60\,k_1}{\nu_1} = 0.102\,(N_{Re_1})^{0.9}\left(1 + \frac{N_{Re_2}}{N_{Re_1}}\frac{\eta_2}{\eta_1}\right)(N_{Sc_1})^{-0.37} \quad , \tag{3}$$

which is similar to Lewis' correlation but includes the Schmidt number. The indicated dependence of the mass transfer coefficient on the molecular diffusivity is 0.37, which lies between the zero dependence maintained by Lewis (corresponding to turbulent mixing) and the exponent of one-half

assumed by Gordon and Sherwood (which corresponds to pure molecular diffusion).

Mayers (8) developed an improved correlation on the basis of Lewis' data and confirmed it by additional experimental data with new systems. The resulting correlation was

$$\frac{k_1 d}{\mathscr{D}_1} = 0.00316 \left(N_{Re_1} N_{Re_2}\right)^{1/2} \left(\frac{n_2}{n_1}\right)^{1.9} \left(0.6 + \frac{n_2}{n_1}\right)^{-2.4} \left(N_{Sc_1}\right)^{5/6} . \qquad (4)$$

Mayers found that the dependence of the film mass transfer coefficient on the molecular diffusivity was one-sixth, placing the process between turbulent mixing and molecular diffusion.

Olander and Benedict (9), who studied the transfer of water into mixtures of tributyl phosphate (TBP) and n-hexane, found that the individual-phase mass transfer coefficient for this system was correlated well by the relation

$$\frac{k_1}{\nu_1} = 0.0134 \left(\frac{N_1}{\nu_1}\right)^{0.67} \left(N_{Sc_1}\right)^{-0.44} . \qquad (5)$$

These authors observed that, below a certain transition speed (which was different for each solvent), the mass transfer coefficient was proportional to the agitator speed to the 0.67 power. At higher speeds, the exponent on the agitator speed changed abruptly to 1.7. This phenomenon is believed to arise from a change in the flow regime in the vicinity of the interface. They also concluded that this change was not necessarily connected with marked visual rippling of the interface.

Olander (10) presented a theoretical model for predicting mass transfer rates in a stirred contactor. In the model he developed, each phase was divided into two parts: the core region (Region I), which contained the liquid in the volume swept out by the stirrer; and an annular region (Region II) between the core and the vessel walls. The expressions Olander developed for the mass transfer coefficient in each region were

$$\text{Region I:} \quad \frac{\overline{k}_c}{\nu} = \left(\frac{9}{20}\alpha\right)^{1/3} \frac{(1 - fc^3)^{2/3}}{(1 - fc^2)} \left(\frac{\omega_\infty}{\nu}\right)^{1/2} (N_{Sc})^{-2/3} \; ; \tag{6}$$

and

$$\text{Region II:} \quad \frac{k_a}{\nu} = \frac{(\alpha/3)^{1/3}}{\Gamma\left(\frac{4}{3}\right)} \frac{(A_C/A_T)^{1/3}}{(1 - A_C/A_T)^{1/3}} \left(\frac{\omega_\infty}{\nu}\right)^{1/2} (N_{Sc})^{-2/3} \; . \tag{7}$$

Good agreement was obtained with Equations (6) and (7) by Loosemore and Prosser (11), who used a cell which substituted a rotating disk above the interface instead of stirrer bars. To test the validity of Equations (6) and (7) separately, portions of the interface were obstructed to prevent mass transfer.

McManamey et al. (12) measured the influence of molecular diffusion on mass transfer rates in a stirred contactor. The systems studied were helium and isobutane transferring from water to toluene and from water to Dekalin, respectively. Their results indicate that the mass transfer coefficient is proportional to the molecular diffusion coefficient raised to the one-half power. A theoretical model was proposed, based on the concept that the total fluctuation velocity in the plane of the liquid-liquid interface is increased when the turbulent fluctuations in both

phases are synchronized (leading to faster mass transfer) and on the assumption that the approach of an eddy to the interface is restrained by interfacial tension and gravitational forces. The expression obtained [which is derived elsewhere (13) in dimensional form] is

$$N_{Sh_1} = C_{(8)} \, (N_{Sc_1})^{0.5} \, (N_{We_1}) \left[N_{Re_1} + \left(\frac{\nu_2}{\nu_1} \right) N_{Re_2} \right]^{0.5} \times$$

$$\left[1 + \frac{\rho_2 \nu_2^2}{\rho_1 \nu_1^2} \left(\frac{N_{Re_2}}{N_{Re_1}} \right)^2 \right]^{0.5} . \qquad (8)$$

In a later study, McManamey et al. (14) confirmed that the mass transfer coefficient in turbulent liquid-liquid systems is proportional to the one-half power of the molecular diffusion coefficient. This work represents an improvement over the previous effort (12), where the equilibrium distribution coefficients were incorrectly measured.

Bulicka and Prochazka (15) developed the following model for turbulent mass transfer in liquid-liquid contactors:

$$N_{Sh_1} = \kappa_g \, N_{Sc_1}^{1/2} \, N_{Re_1}^{3/4} \, \Psi_{1,2} , \qquad (9)$$

where Ψ is a factor which accounts for the effects of turbulence in one phase (phase 2) on mass transfer rates in the other phase (phase 1). Equation (9) was developed on the basis that surface renewal occurs by turbulent disturbances and unsteady mass transfer takes place by molecular diffusion into the elementary vortices.

It is apparent that a great deal of research has been performed with nondispersing contactors to elucidate the basic mechanisms of mass

transfer which can be expected to occur. Very little information is available, however, concerning mass transfer occurring between fluids with widely varying physical properties such as the fluids used in the processes cited earlier. Data are also lacking on the variation of mass transfer coefficient with parameters such as agitator diameter, phase volumes, and cell size, which are important in scale-up operations. This research effort was therefore directed toward measuring mass transfer rates as a function of fluid physical properties and the cell geometry parameters that have not been studied previously.

CHAPTER III

THEORY OF POLAROGRAPHY

A polarographic method for measuring mass transfer rates was adapted to the nondispersing contactor system. This method has several desirable characteristics, the foremost of which is that the location of the measured mass transfer resistance is known. The technique is also very rapid and permits acquisition of a large amount of data in the same period of time that would be required to perform one test using the mutual solubility technique.

The polarographic technique for determining aqueous-phase mass transfer coefficients involves oxidation of a reduced species or reduction of an oxidized species at an electrode, which is at a condition of concentration polarization. Concentration polarization is noted when the concentration of the reacting species decreases from the bulk solution value to essentially zero across a thin stagnant layer near the electrode surface.

One system that has been studied previously (16) is the reduction of ferricyanide ions at a polarized nickel electrode. As ferricyanide was reduced at the cathode, ferrocyanide was oxidized at the anode. There was no net consumption of chemicals or change in the composition of the electrolyte solution.

Polarization of the cathode can be accomplished in one of two ways--either the cathode surface area is made very large with respect to the anode surface area, or the concentration of the oxidized species is made very small with respect to the reduced species.

The migration of an ion in both electric and concentration fields is described by the Nernst-Planck equation

$$Q = \mathscr{D}(\nabla C + \frac{ZCF}{RT} \nabla \Phi) \ , \qquad (10)$$

where

Q = flux of the ion, kg-moles/m^2-sec,

$\mathscr{D}$ = diffusion coefficient, m^2/sec,

C = concentration of reacting ion, kg-moles/m^3,

Z = valence change of the transferring ion, equiv/kg-mole,

F = Faraday constant, coul/kg-mole,

R = gas constant, joules/kg-mole-K,

T = absolute temperature, K,

Φ = electric potential, V.

The first and second terms in the expression represent the contribution of ordinary diffusion to the flux and the contribution of electromigration, respectively. A large concentration (relative to that of the reacting ion) of an inert electrolyte alters the dielectric properties of the solution such that the potential will decrease smoothly across the region between the electrodes, while the concentration drops sharply across the thin polarized layer near the cathode. Thus, the term containing the electric potential becomes relatively small, and

$$Q \approx \mathscr{D} \nabla C \ . \qquad (11)$$

The current flowing between the electrodes is therefore a measure of mass transfer rates governed by ordinary molecular diffusion. For this reason, it is sometimes called the "diffusion current."

The total molar flow rate of ions to the interface is given by the product of the concentration driving force, the mass transfer coefficient,

and the interfacial area available for mass transfer:

$$J = kA(C_B - C_i) \ , \tag{12}$$

where

J = molar flow rate of ions,

k = film mass transfer coefficient,

A = interfacial area,

C_B = bulk concentration of ions, and

C_i = interfacial concentrations of ions.

Rearranging yields

$$k = \frac{J}{A(C_B - C_i)} \ , \tag{13}$$

but

$$J = \frac{I}{ZF} \tag{14}$$

and $C_i = 0$ since the interface is the polarized electrode; therefore, Equation (13) becomes

$$k = \frac{I}{(Z)(F)(A)(C_B)} \ . \tag{15}$$

This relates the experimentally obtainable quantities I, A, and C_B to the mass transfer coefficient through the electrolyte film.

CHAPTER IV

APPARATUS AND PROCEDURE

Apparatus for Mass Transfer Coefficient Measurements

A schematic diagram of the experimental apparatus is shown in Figure 2. The contactor vessels are Plexiglas boxes of square cross section, with a depth/width ratio of 2. The agitators are flat four-bladed turbines with one turbine centered in each phase. The anodes for each cell are made from 1.6-mm-thick brass sheet formed to fit the inner perimeter of the cell and suspended in the aqueous phase. The anodes are plated with gold or silver to resist chemical attack by the aqueous solution.

The potential of the mercury surface relative to a saturated calomel electrode (SCE) suspended in the aqueous phase is controlled while current is passed between the anode and the cathode. A potentiostat capable of automatically varying the impressed voltage between limits of +2 V (SCE) and -2 V (SCE) at rates up to 1 V/min is used. The current through the cell is plotted versus the mercury surface potential on a Hewlett-Packard X-Y plotter.

Procedure for Mass Transfer Coefficient Measurements

The composition of the aqueous phase for the runs made in this study ranged from 0.01 to 0.05 M hydroquinone and from 0.0002 to 0.001 M quinone, in a 0.2 M phosphate buffer solution with a pH of 7.0. The mercury used for the heavy phase was obtained from the Analytical Chemistry Division at ORNL.

The cell was filled with an appropriate volume of each phase, and the turbines were positioned at the midpoint of each phase. The aqueous

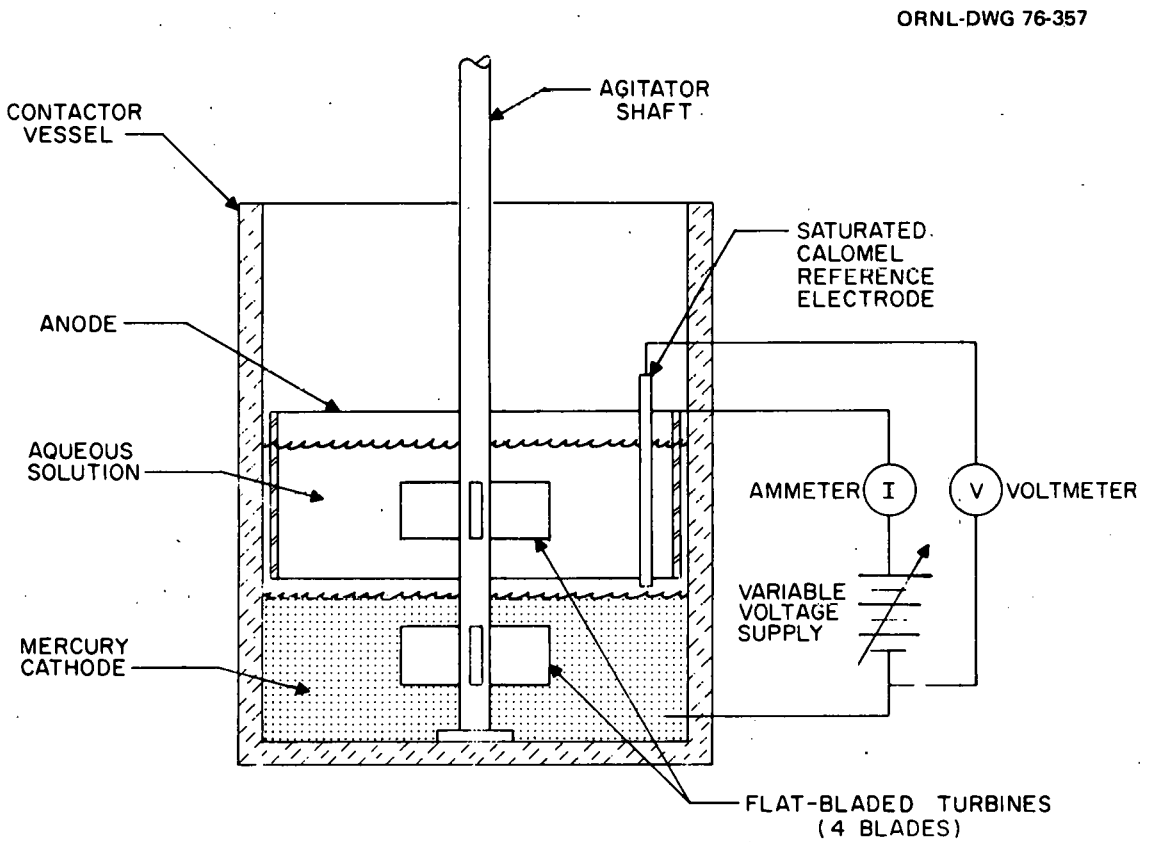

Figure 2. Schematic Diagram of Equipment Used for Measuring Mass Transfer Coefficients in the Stirred Aqueous-Mercury Cell.

phase was subsequently sparged with argon to remove dissolved air. A small bleed of argon was maintained through the vapor space above the electrolyte during each experiment to prevent introduction of oxygen. The agitator drive was then started and adjusted to the desired speed. The voltage between the mercury and the SCE was changed from 0 to -1.4 V, and the cell current and voltage were automatically recorded on the X-Y plotter by the potentiostat. At this point, the agitator speed was adjusted to another value, and the procedure was repeated until a satisfactory range of agitator speeds had been investigated. The entire sequence of steps was performed under photographic-safe lights to prevent deterioration of the electrolyte due to exposure to ultraviolet radiation.

A typical current-voltage recording is shown in Figure 3. The cell current is recorded over the range of 0 to -1.4 V versus SCE at different agitator speeds. At each speed, the cell current rises with increasing voltage at low voltages but reaches a constant value at higher voltages. This constant-current plateau is the diffusion-limited current of interest, which is due to the reversible reduction of quinone at the mercury surface represented by

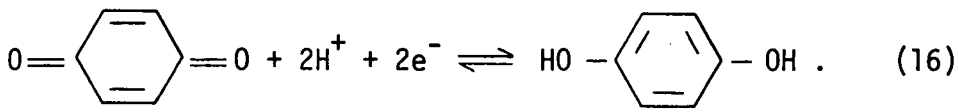

(16)

The diffusion current actually oscillates about an average value because of turbulent fluctuation at the interface. This value, which can be obtained from the recordings, is the basis for determination of the mass transfer coefficient using Equation (15).

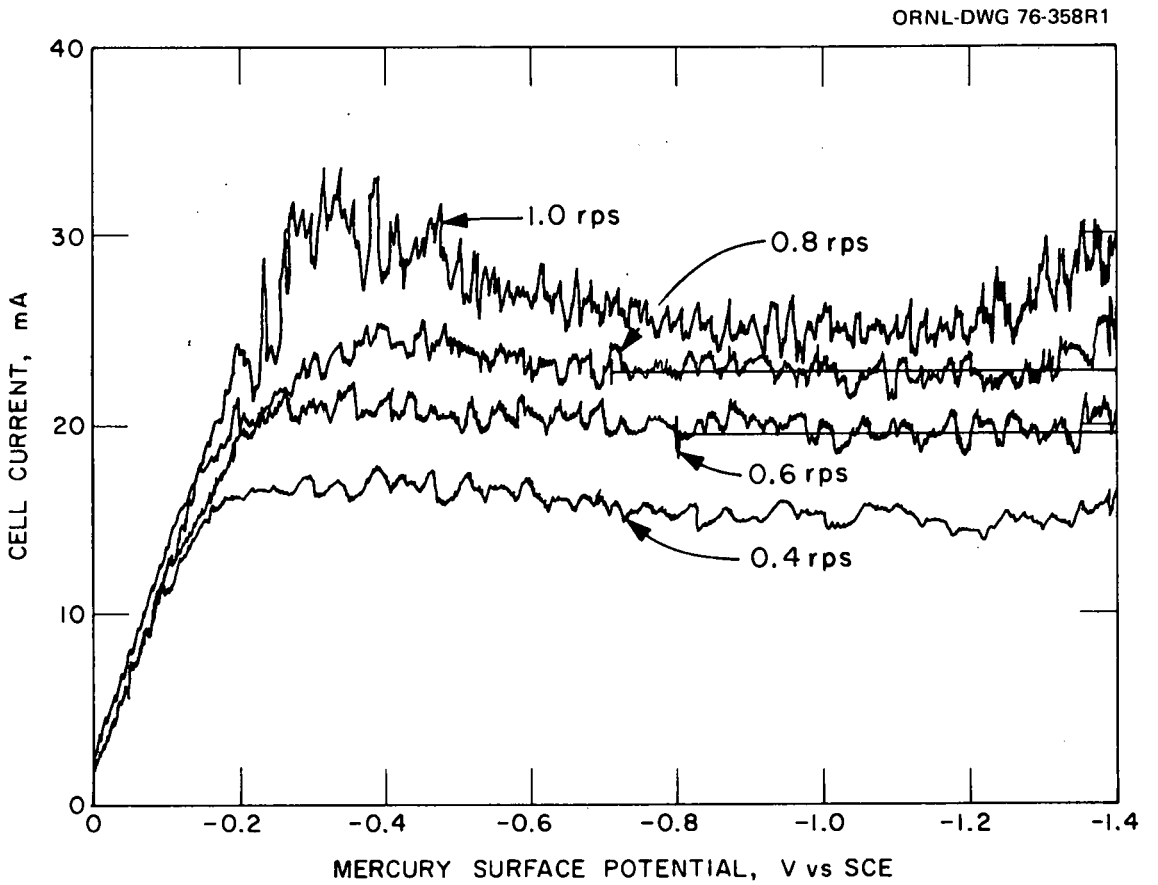

Figure 3. Typical Current-Voltage Recording for Measurement of Mass Transfer Coefficients in the Aqueous-Mercury Cell.

Apparatus and Procedure for Measuring Quinone Diffusion Coefficients

Measurement of the diffusion coefficient of quinone in the electrolyte medium was desirable in order to facilitate correlation of the mass transfer coefficient data. A d.m.e. apparatus provided by the ORNL Analytical Chemistry Division was used for this purpose. This apparatus has been described in detail by Kolthoff and Lingane (17).

The d.m.e. was calibrated by preparing a standard solution of known concentrations of both quinone and hydroquinone in a phosphate buffer. The aqueous viscosity was varied by the addition of sucrose. Composite cathodic-anodic waves were then measured with the standard solutions and with dilutions of the standard solution with water. A typical cathodic-anodic wave, shown in Figure 4, is similar to those presented in the literature (17). The hydroquinone oxidation wave starts at 0.2 V versus SCE (abscissca of Figure 3) and continues to approximately 0.15 V versus SCE. In this region, the current (ordinate of Figure 4) is limited by the diffusion rate of hydroquinone to the mercury surface where it is oxidized to quinone. The curve then increases rapidly to a second region where the current increases only slightly with increasing potential. In this region ($\sim$ 0.0 to -0.4 versus SCE), the current is limited by the rate of diffusion of quinone to the mercury surface where it is reduced to hydroquinone. The diffusion-limited current is determined graphically by the intersection of a tangent line through the zero-current portion of the wave and tangent lines through each of the diffusion-limited plateaus. The intersection points are labeled A and B in Figure 4. The distance from zero on the abscissa to point A corresponds to the diffusion current

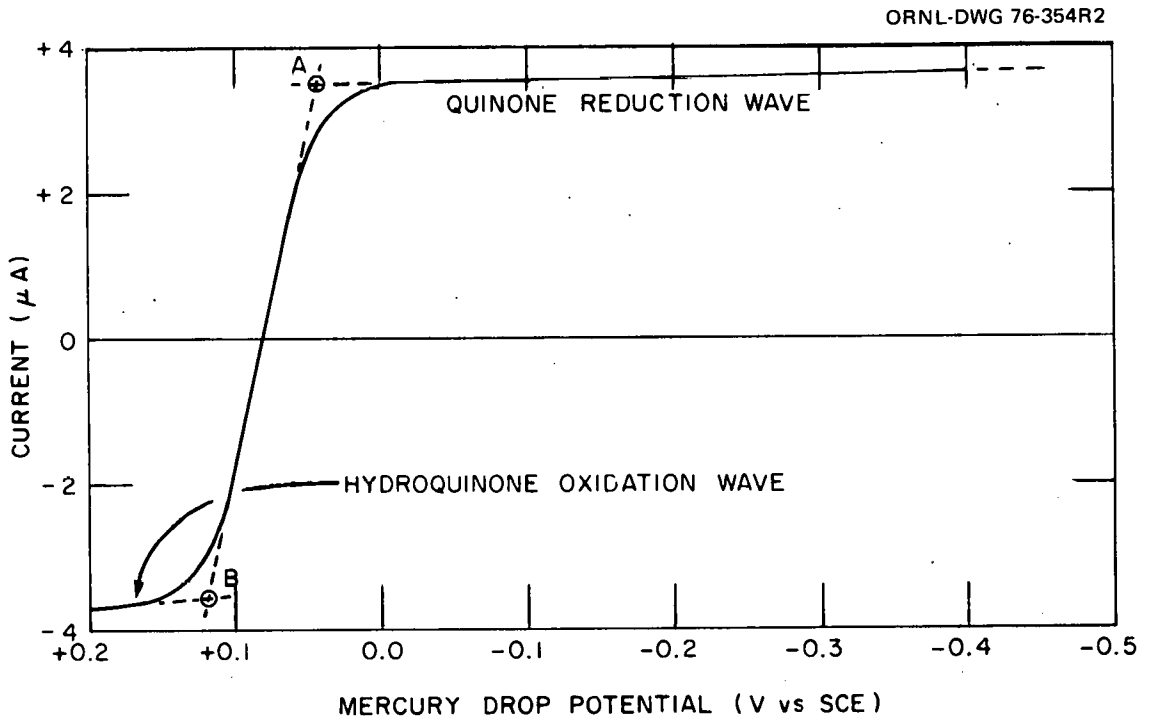

Figure 4. Composite Oxidation-Reduction Wave of 0.001 M Quinone and Hydroquinone in 0.001 M Phosphate Buffer (pH = 7) at the Dropping Mercury Electrode.

of quinone, while the distance from point B to zero on the abscissa represents the diffusion current of hydroquinone.

The measured diffusion current, the quinone bulk concentration, and several apparatus parameters were used to calculate the quinone diffusion coefficient via the following semiempirical equation (18):

$$I_o = 607\ B\mathscr{D}^{1/2} C\ M^{2/3}\ t^{1/6} \left(1 + \frac{39\mathscr{D}^{1/2}\ t^{1/6}}{M^{1/3}}\right), \qquad (17)$$

where

I_o = current averaged over the lifetime of a mercury drop, mA;

B = number of Faradays of electricity required per mole of electrode reaction;

$\mathscr{D}$ = diffusion coefficient, cm^2/sec;

C = bulk concentration of diffusing species, millimoles/liter;

M = mercury flow rate, mg/sec;

t = mercury drop time, sec.

Equation (17) was used to determine the diffusion coefficient of quinone in each combination of aqueous quinone and sucrose concentrations.

CHAPTER V

EXPERIMENTAL DATA

The experimental data can be divided into three groups: the aqueous film mass transfer coefficients measured as a function of the system variables, the quinone diffusion coefficient measured as a function of the aqueous-phase physical properties, and measurement of the aqueous-phase viscosity and density. These data are presented in the following three sections.

Mass Transfer Coefficient for the Electrolyte Film

A summary of the range of experimental parameters is presented in Table 1. Three cells, with base dimensions of 0.102, 0.203, and 0.305 m, respectively, were used. Three to five different agitator diameters ranging from 0.038 to 0.280 m were tested for each cell size. Two or three phase volumes varying between 0.0007 and 0.018 m^3 were tested for each combination of cell size and agitator diameter. Three different aqueous-phase sucrose concentrations, 0, 34, and 45 wt %, were investigated for each combination of cell size, agitator diameter, and phase volume. Finally, for each set of experimental parameters listed above, mass transfer coefficients were measured over the range of agitator speeds listed in Table 1.

The mass transfer coefficients measured as a function of agitator rotational speed are shown in Figures 5 through 23. Figures 24 through 29 show the variation of the mass transfer coefficient with various system parameters held constant. Figure 30 illustrates the effect of agitating each phase independently on the mass transfer coefficient.

Table 1. Summary of Experimental Parameters for Measurement of Aqueous-Phase Mass Transfer Coefficients

Cell Size (m x m)	Agitator Diameter (m)	Phase Volumes (m^3)	Aqueous-Phase Sucrose Concentration (wt %)	Range of Agitator Speeds (rps)
0.102 x 0.102	0.038	0.0007, 0.0009	34, 45	0.33 - 3.67
	0.064	0.0007, 0.0009	0, 34, 45	0.27 - 2.32
	0.089	0.0007, 0.0009	0, 34, 45	0.32 - 1.87
0.203 x 0.203	0.089	0.003, 0.005, 0.007	0, 34, 45	0.33 - 2.40
	0.140	0.003, 0.005, 0.007	0, 34, 45	0.33 - 2.00
	0.190	0.003, 0.005, 0.007	0, 34, 45	0.28 - 1.35
0.305 x 0.305	0.089	0.009, 0.018	0	0.48 - 3.13
	0.140	0.009, 0.018	0	0.33 - 2.33
	0.190	0.009, 0.018	0, 34, 45	0.33 - 1.67
	0.240	0.009, 0.018	0, 34, 45	0.33 - 1.33
	0.280	0.009, 0.018	0, 34, 45	0.27 - 1.00

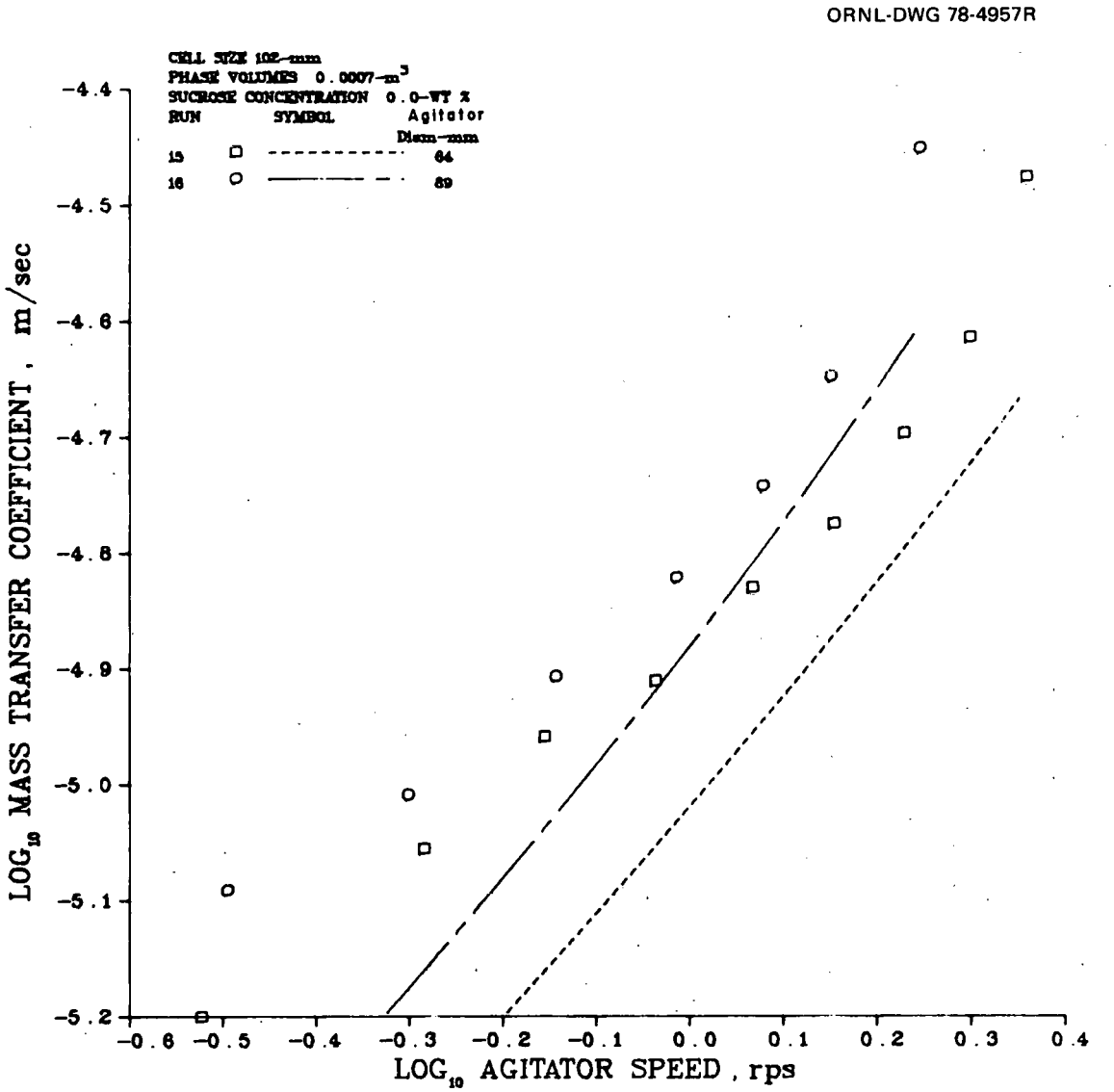

Figure 5. Mass Transfer Coefficient Versus Agitator Speed for Runs 15 and 16.

ORNL-DWG 78-4958R

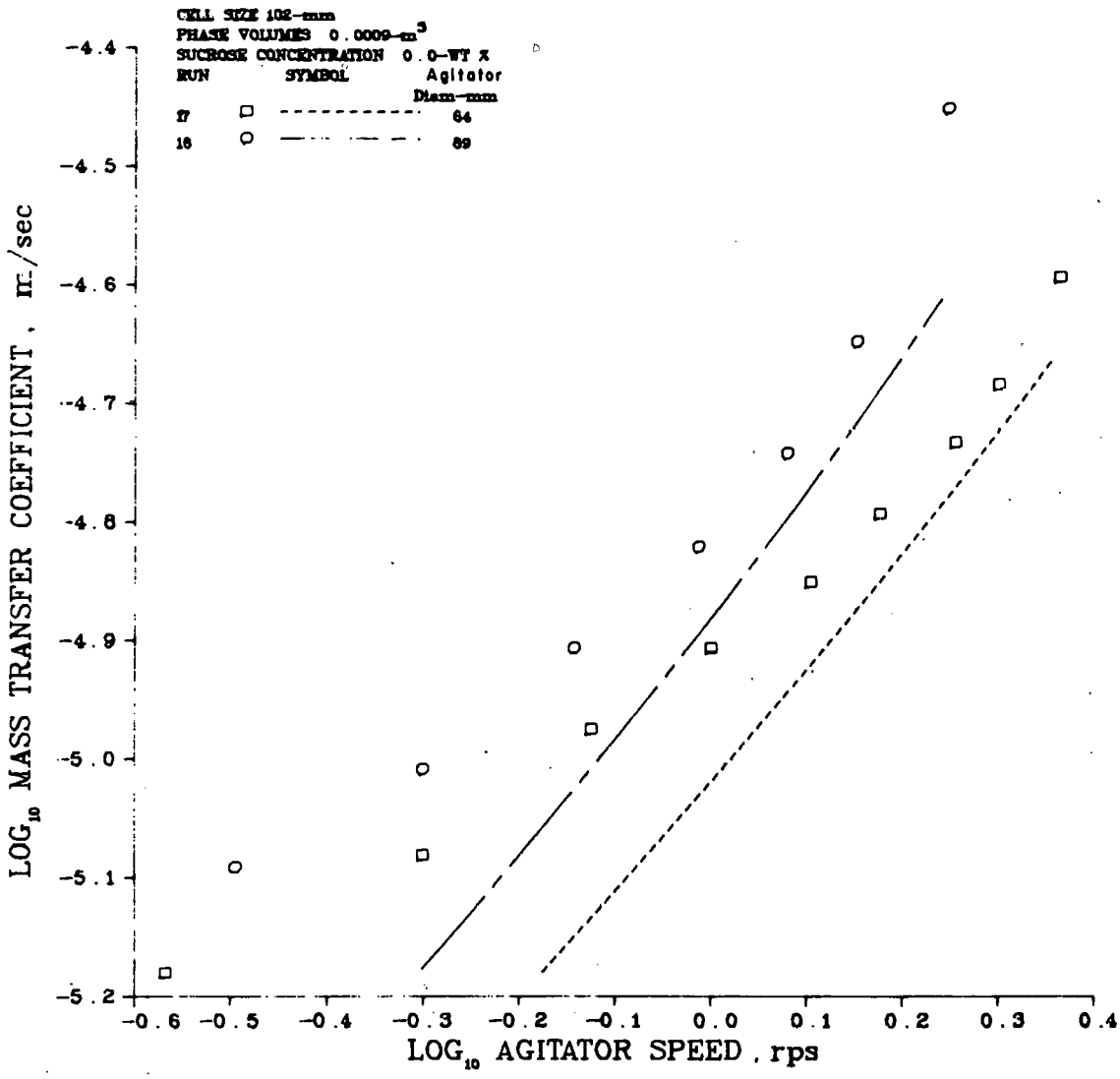

Figure 6. Mass Transfer Coefficient Versus Agitator Speed for Runs 17 and 18.

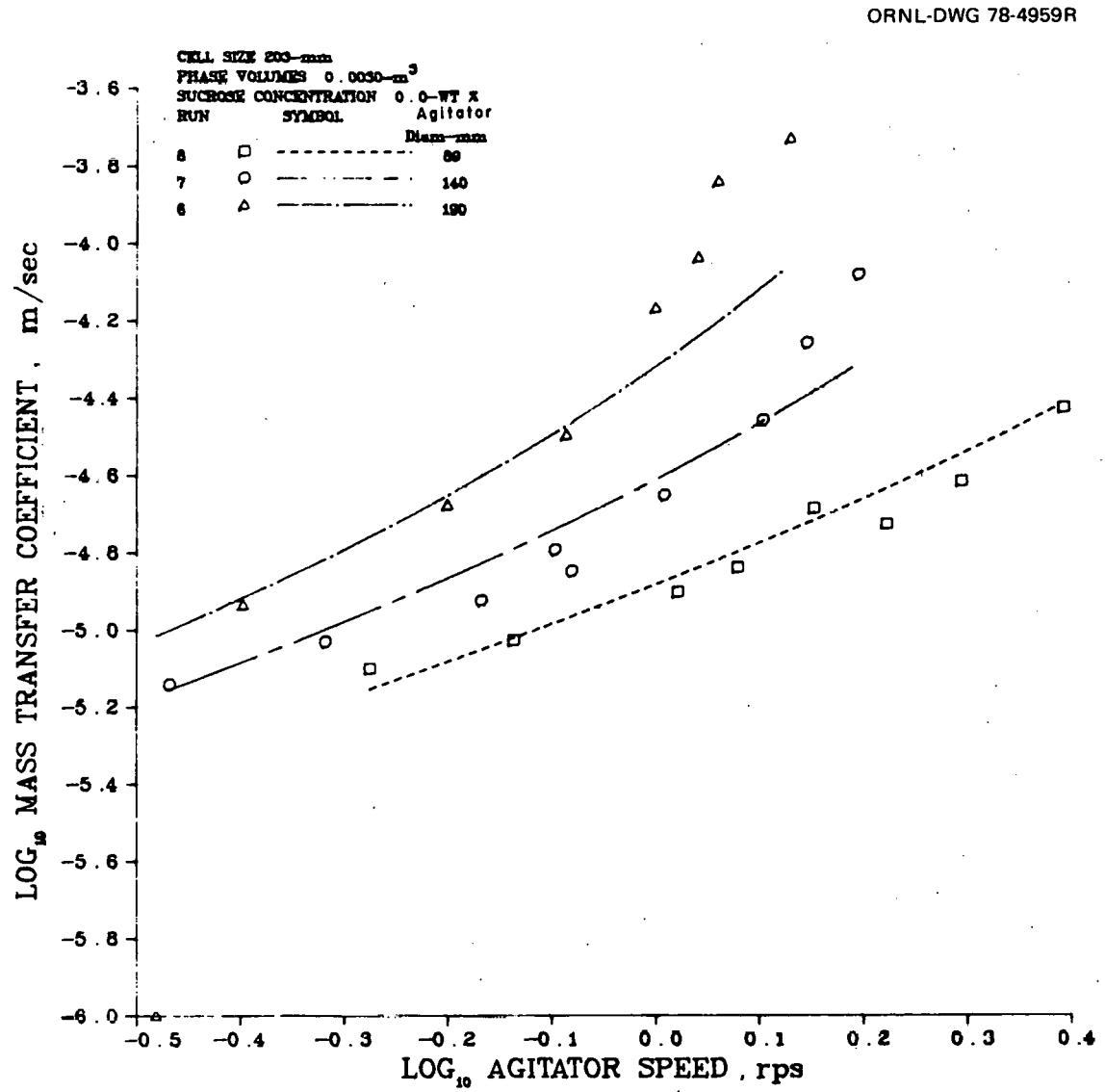

Figure 7. Mass Transfer Coefficient Versus Agitator Speed for Runs 8, 7, and 6.

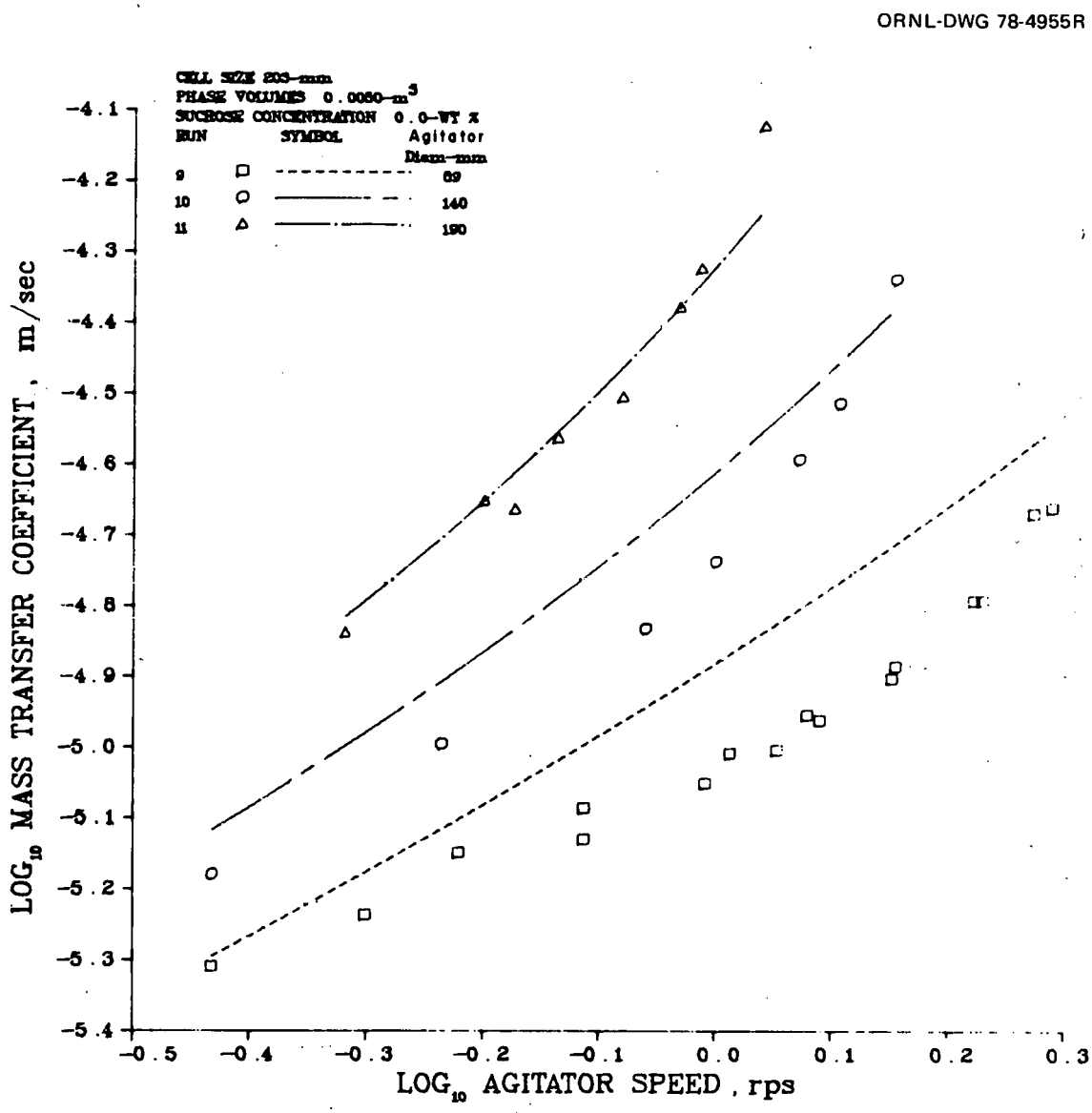

Figure 8. Mass Transfer Coefficient Versus Agitator Speed for Runs 9, 10, and 11.

ORNL-DWG 78-4956R

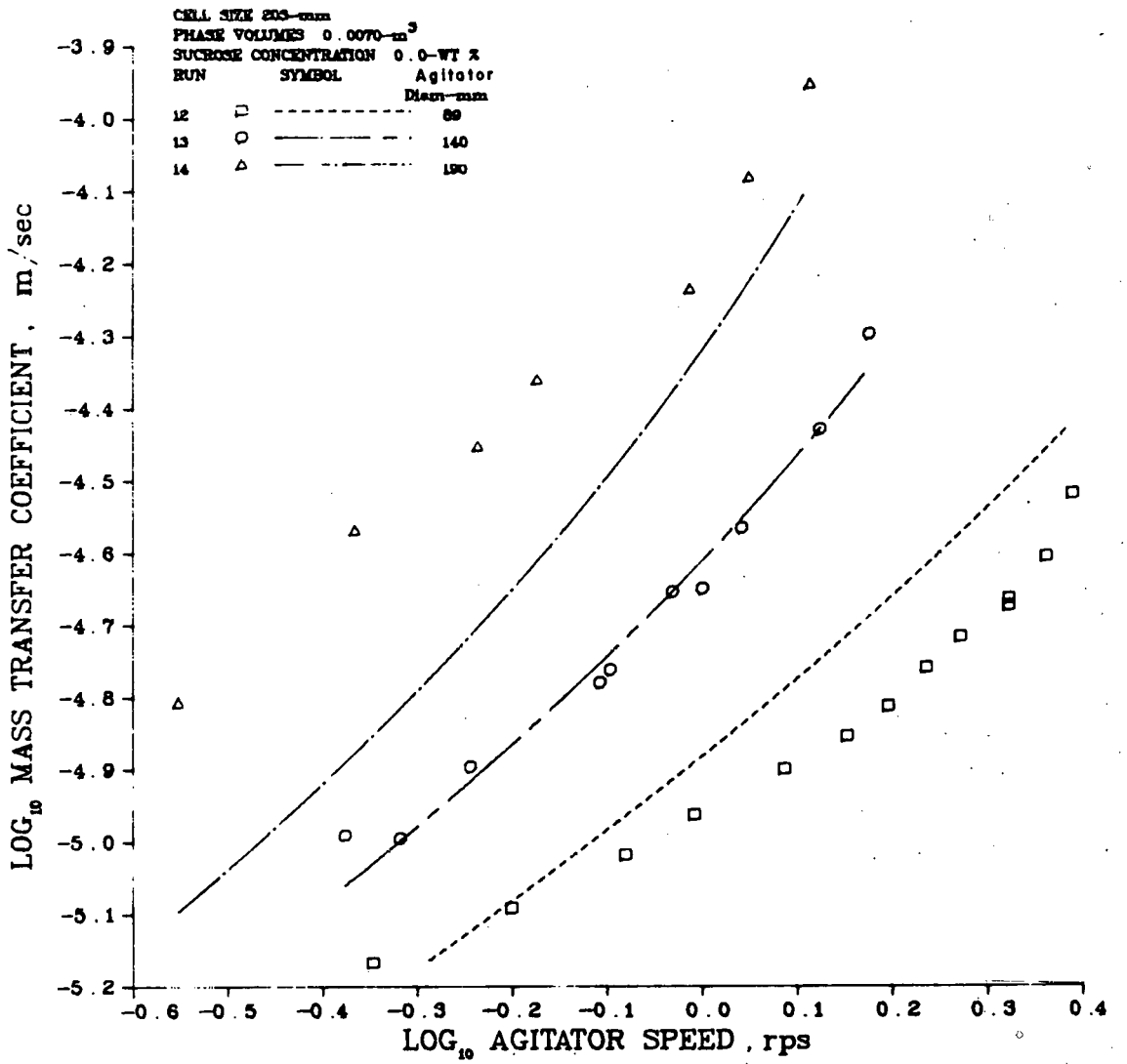

Figure 9. Mass Transfer Coefficient Versus Agitator Speed for Runs 12, 13, and 14.

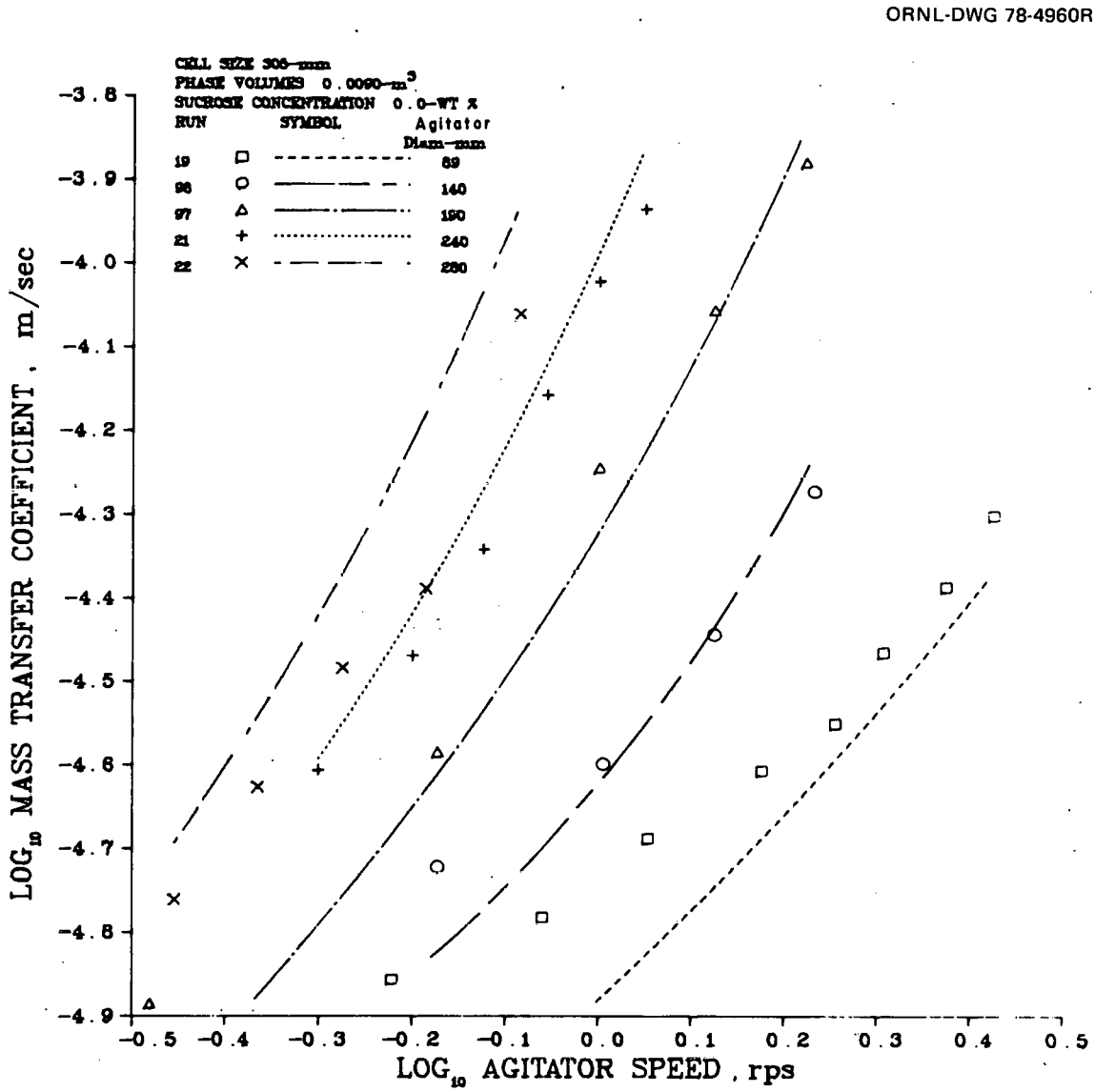

Figure 10. Mass Transfer Coefficient Versus Agitator Speed for Runs 19, 98, 97, 21, and 22.

ORNL-DWG 78-4961R

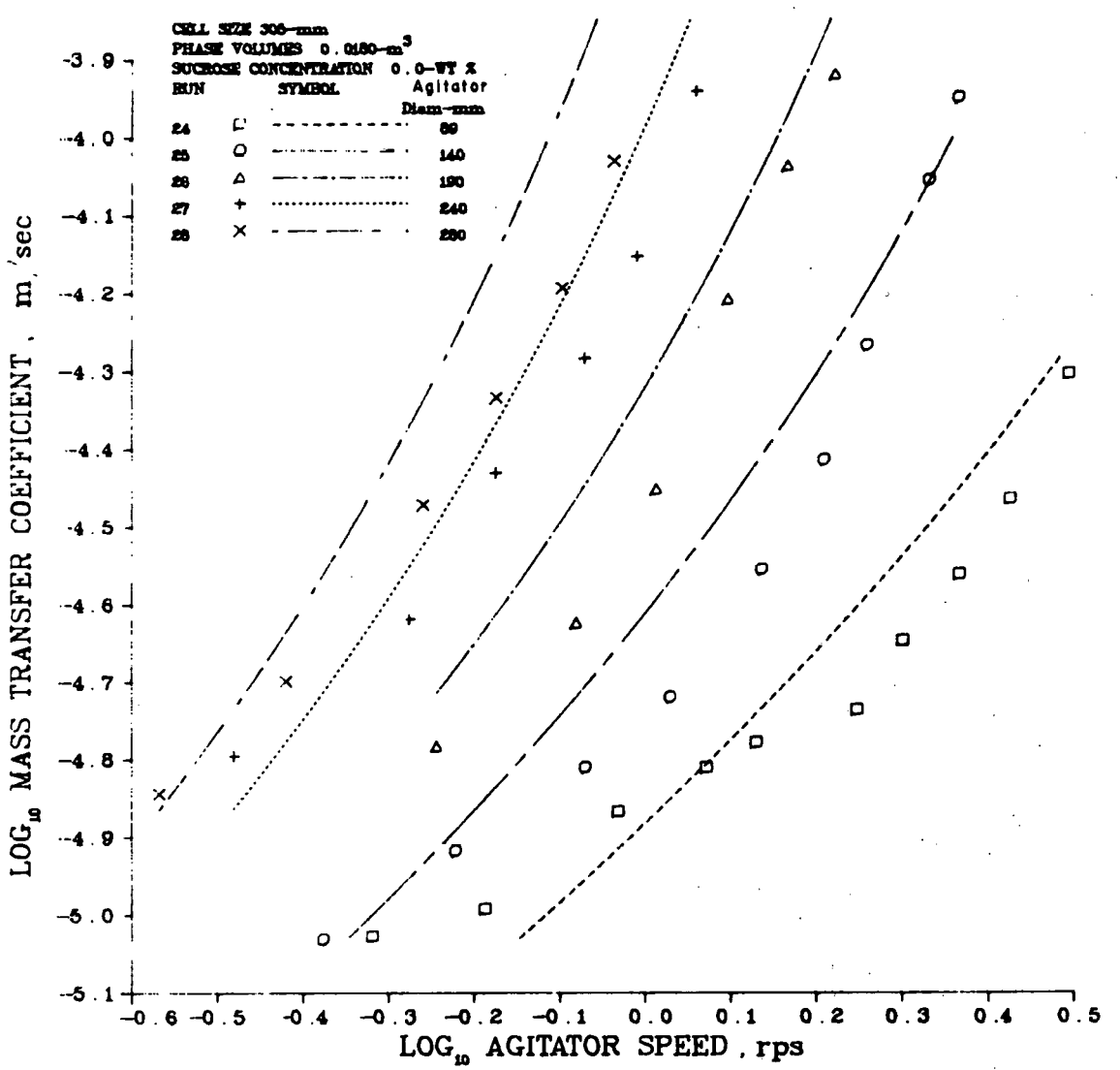

Figure 11. Mass Transfer Coefficient Versus Agitator Speed for Runs 24, 25, 26, 27, and 28.

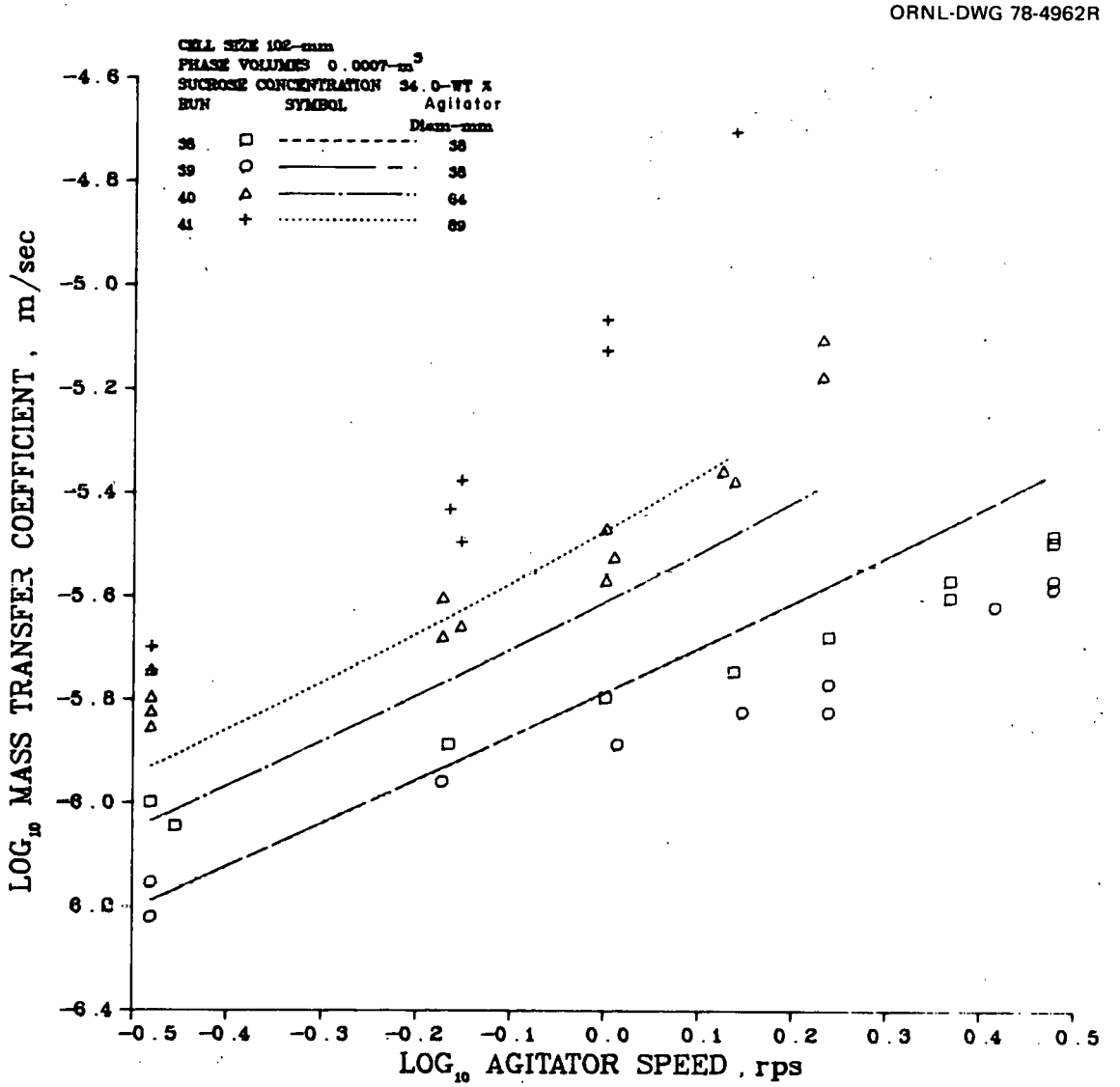

Figure 12. Mass Transfer Coefficient Versus Agitator Speed for Runs 38, 39, 40, and 41.

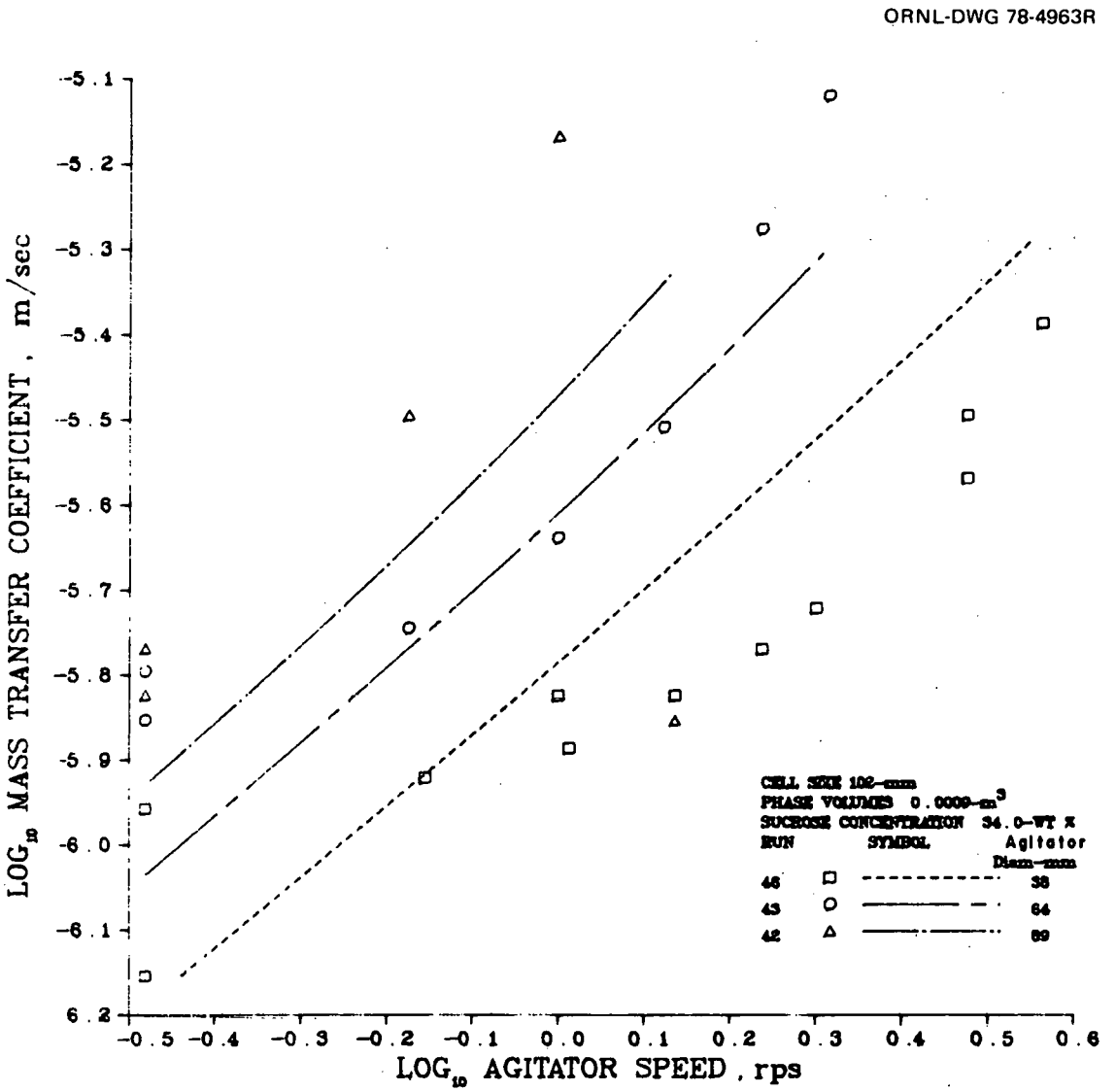

Figure 13. Mass Transfer Coefficient Versus Agitator Speed for Runs 46, 43, and 42.

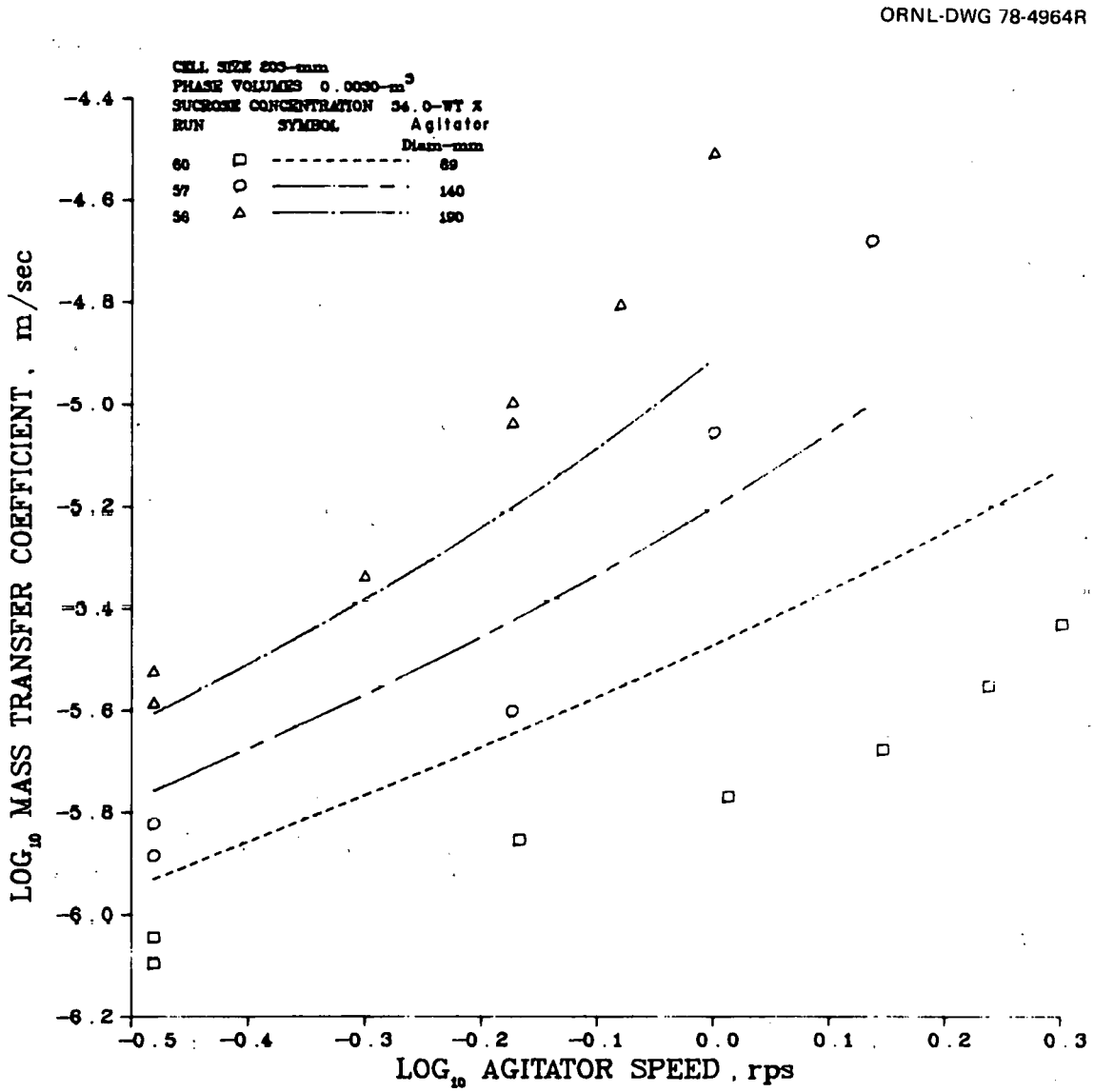

Figure 14. Mass Transfer Coefficient Versus Agitator Speed for Runs 60, 57, and 56.

ORNL-DWG 78-4965R

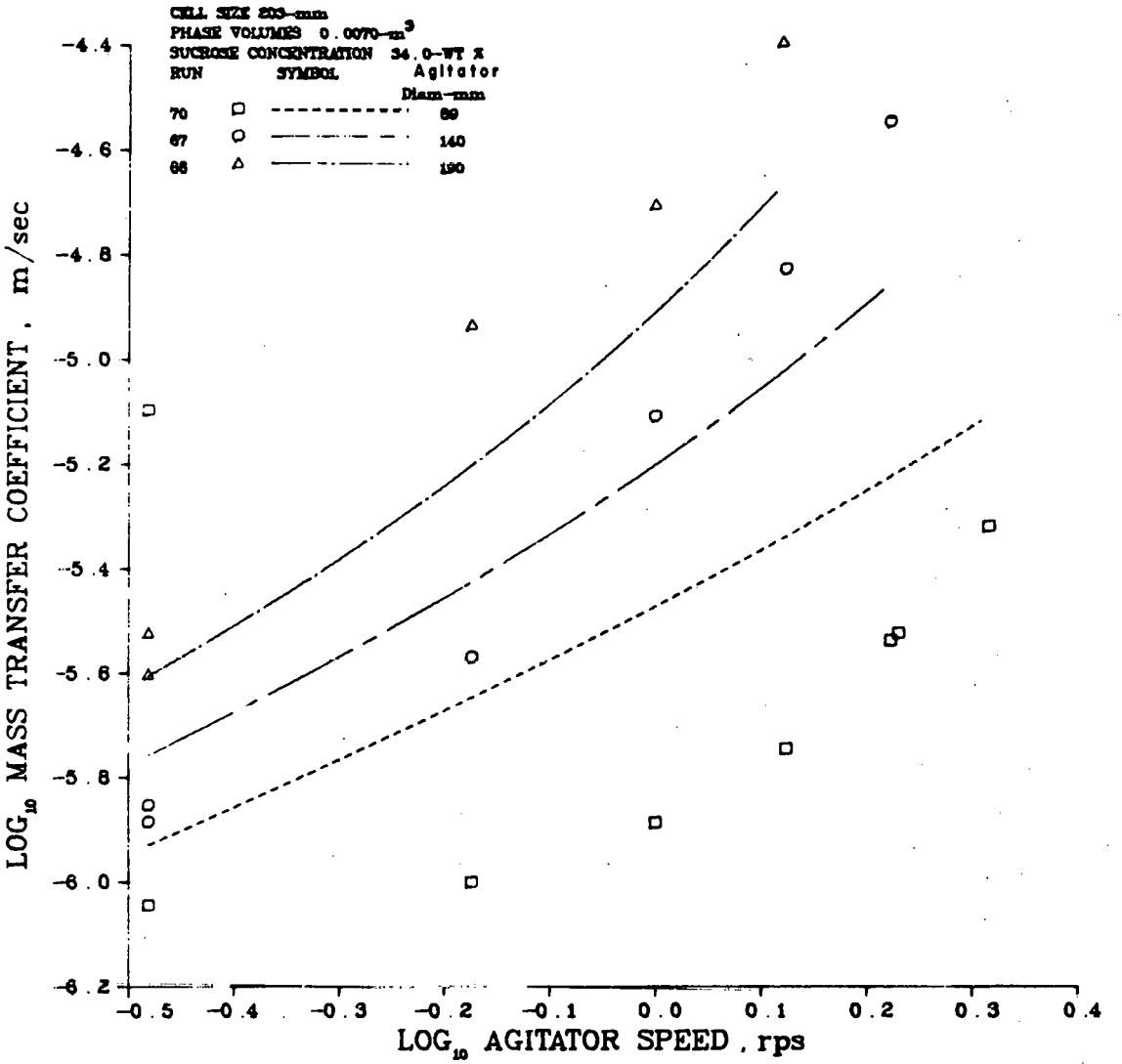

Figure 15. Mass Transfer Coefficient Versus Agitator Speed for Runs 70, 67, and 66.

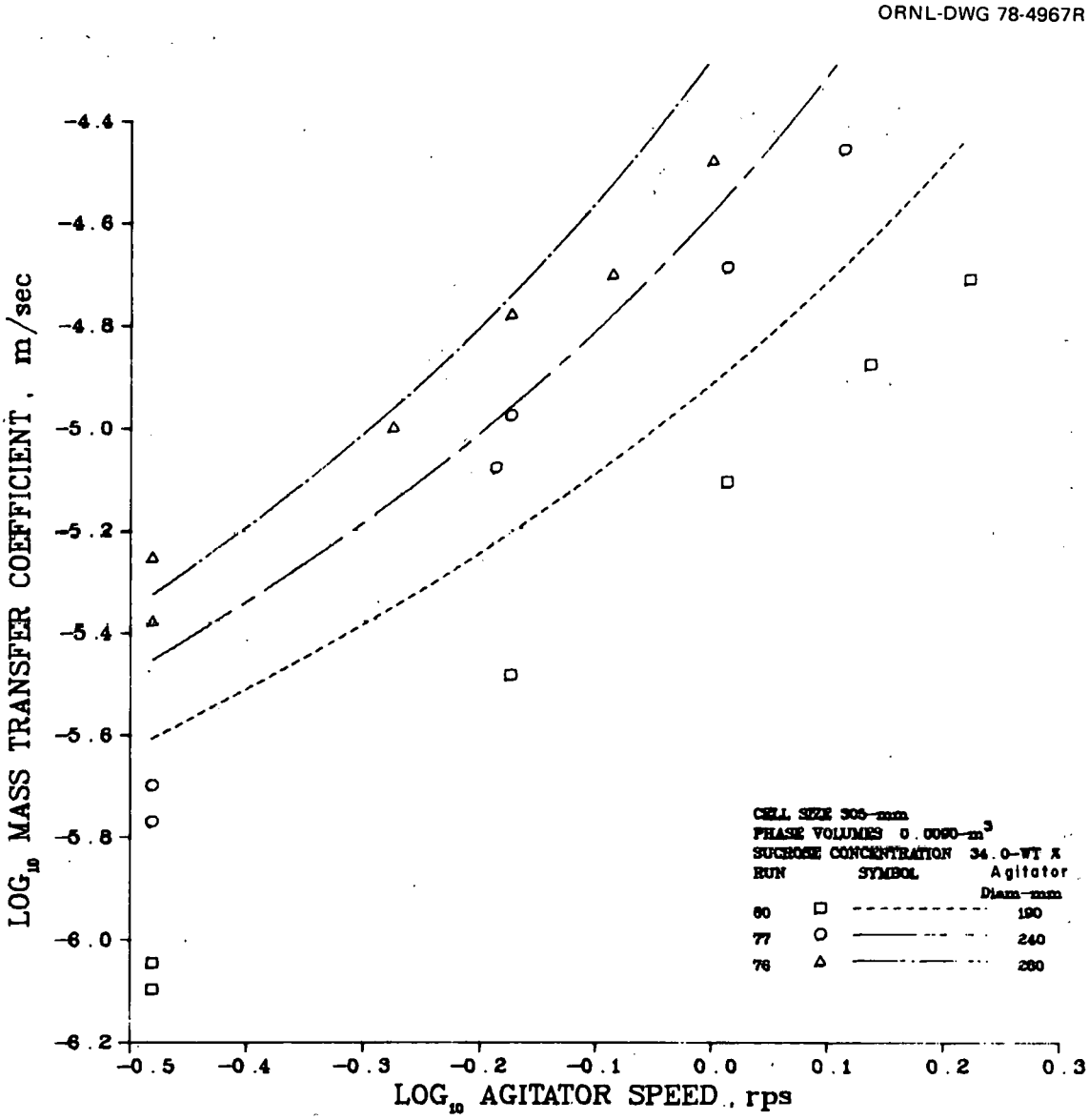

Figure 16. Mass Transfer Coefficient Versus Agitator Speed for Runs 80, 77, and 76.

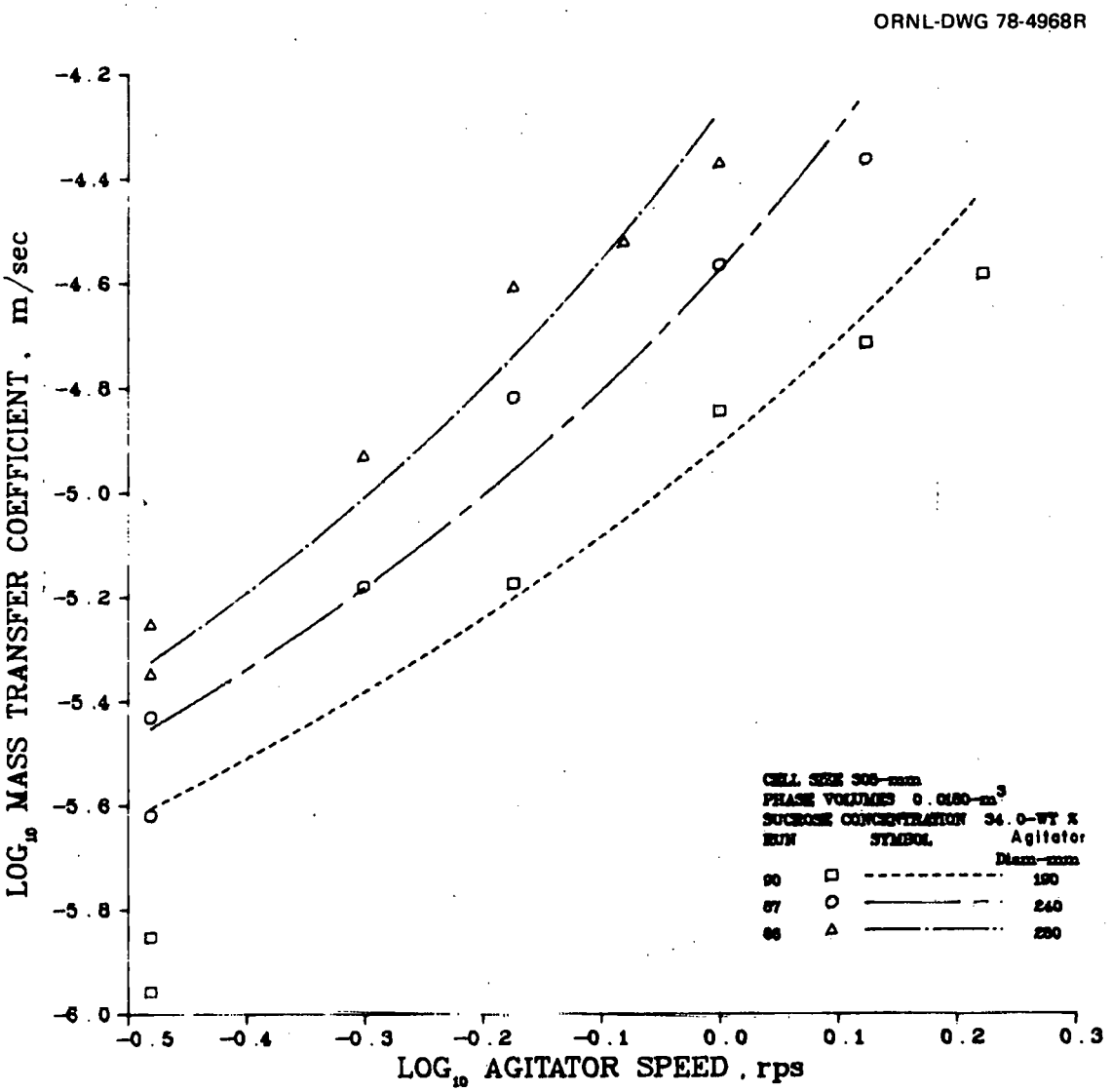

Figure 17. Mass Transfer Coefficient Versus Agitator Speed for Runs 90, 87, and 86.

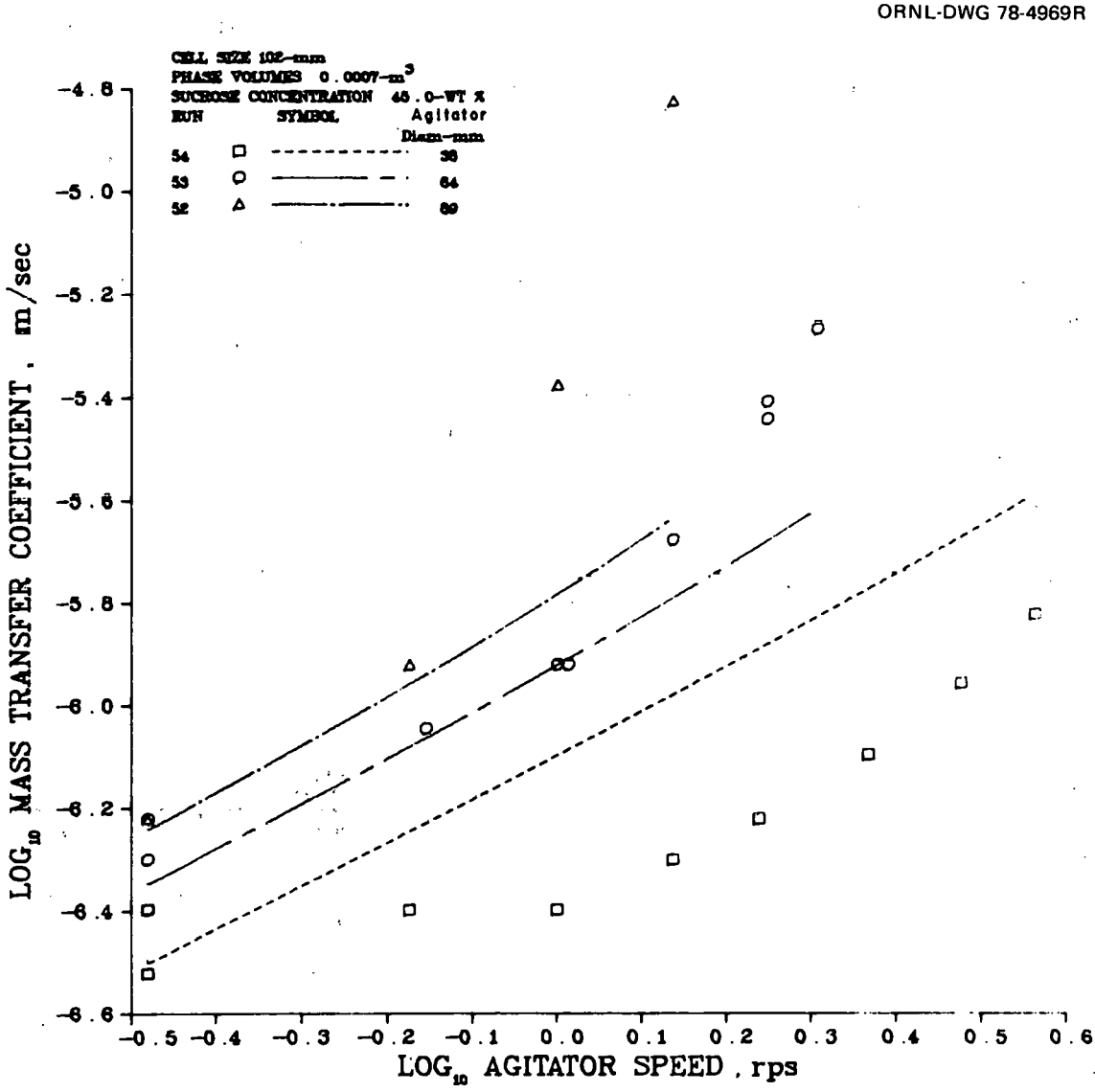

Figure 18. Mass Transfer Coefficient Versus Agitator Speed for Runs 54, 53, and 52.

ORNL-DWG 78-4970R

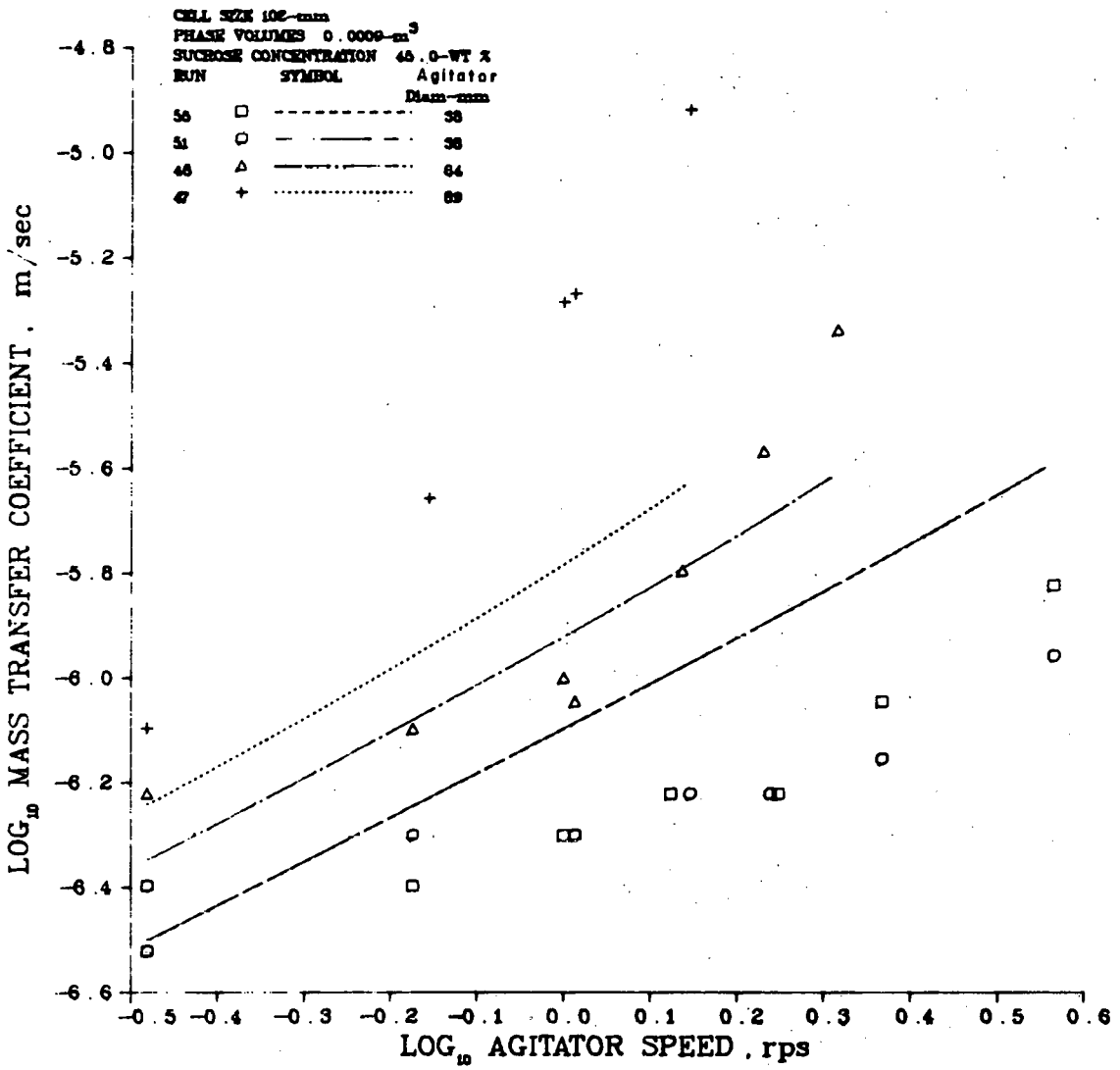

Figure 19. Mass Transfer Coefficient Versus Agitator Speed for Runs 55, 51, 48, and 47.

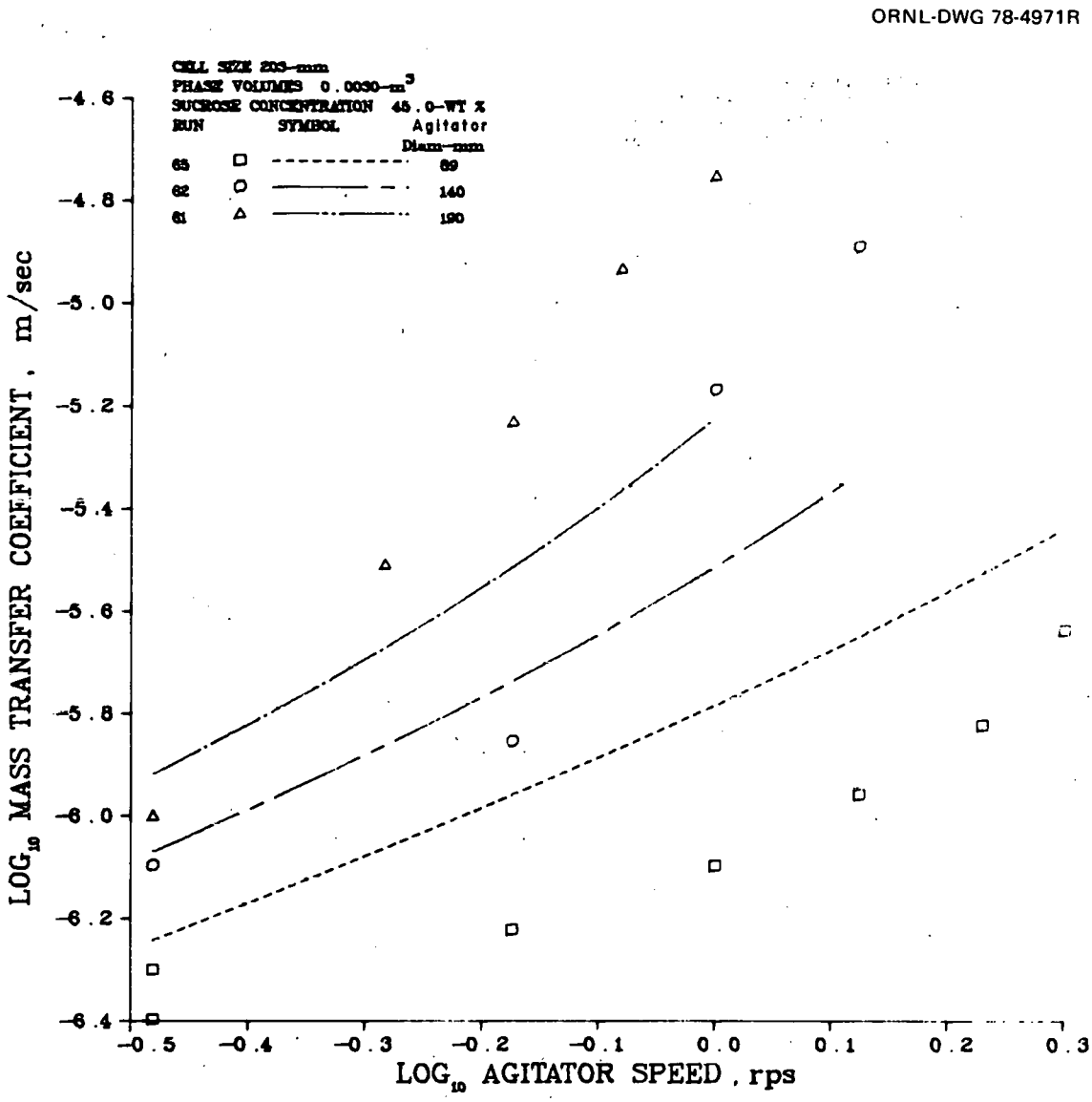

Figure 20. Mass Transfer Coefficient Versus Agitator Speed for Runs 65, 62, and 61.

ORNL-DWG 78-4972R

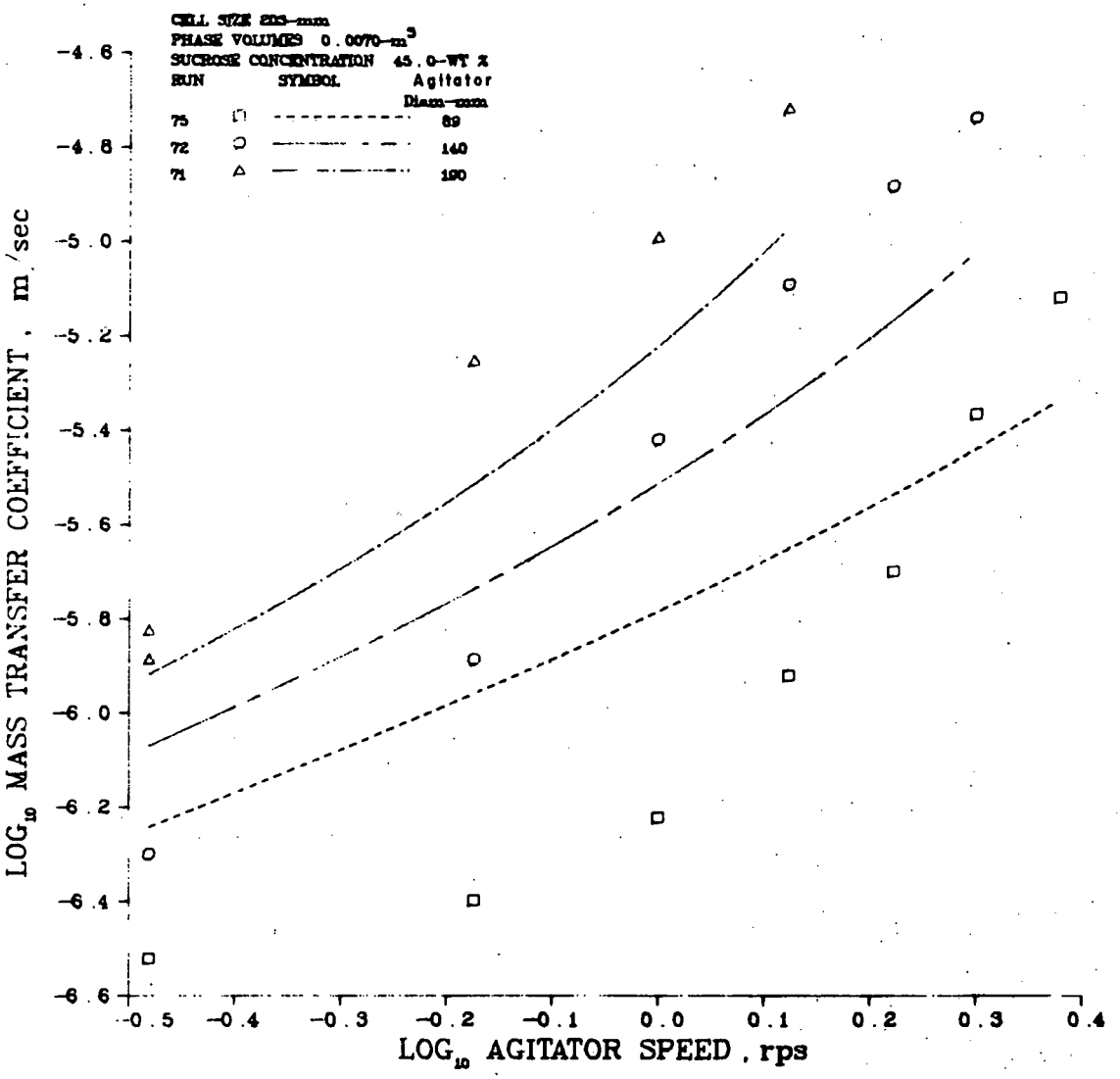

Figure 21. Mass Transfer Coefficient Versus Agitator Speed for Runs 75, 72, and 71.

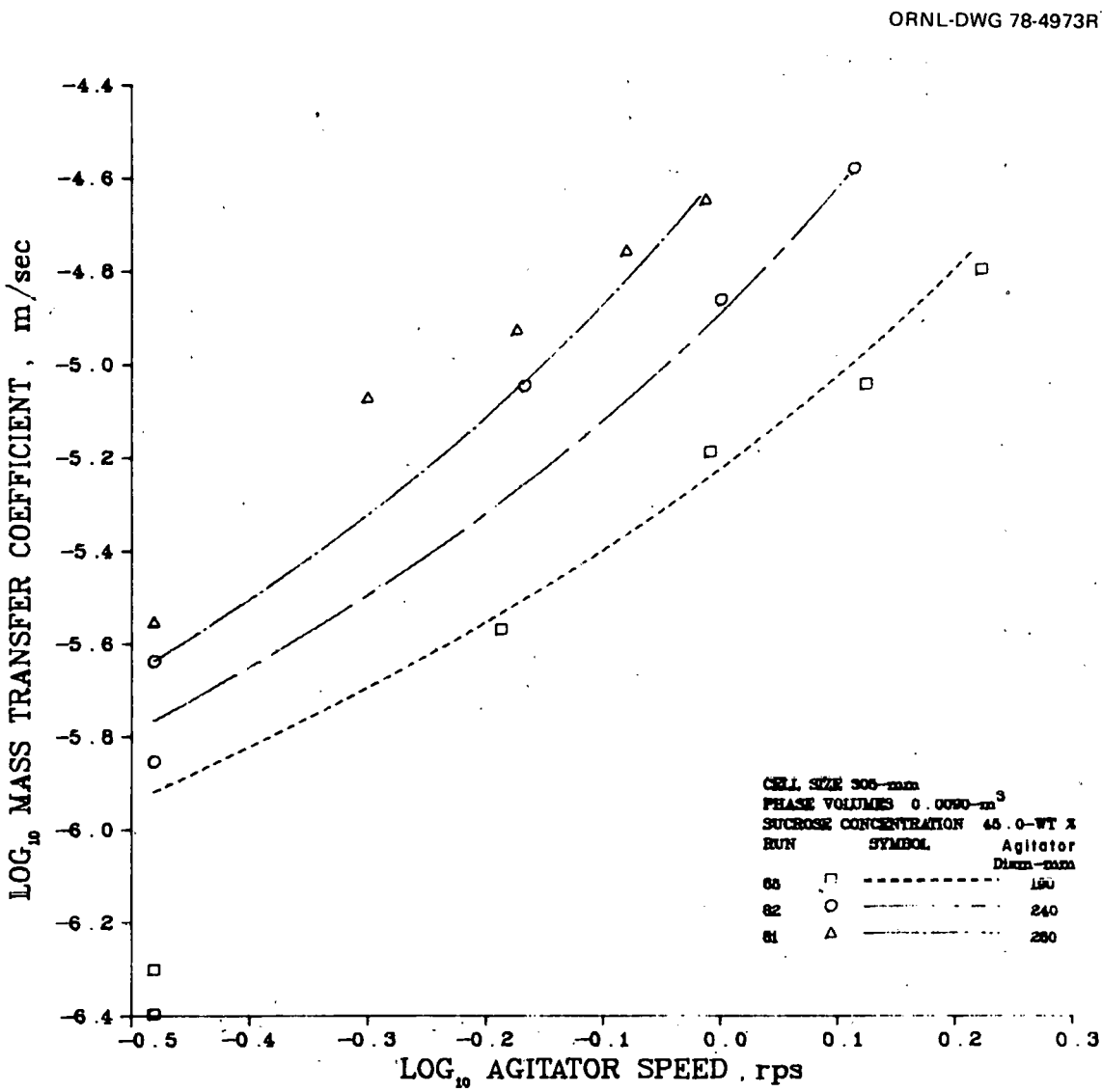

Figure 22. Mass Transfer Coefficient Versus Agitator Speed for Runs 85, 82, and 81.

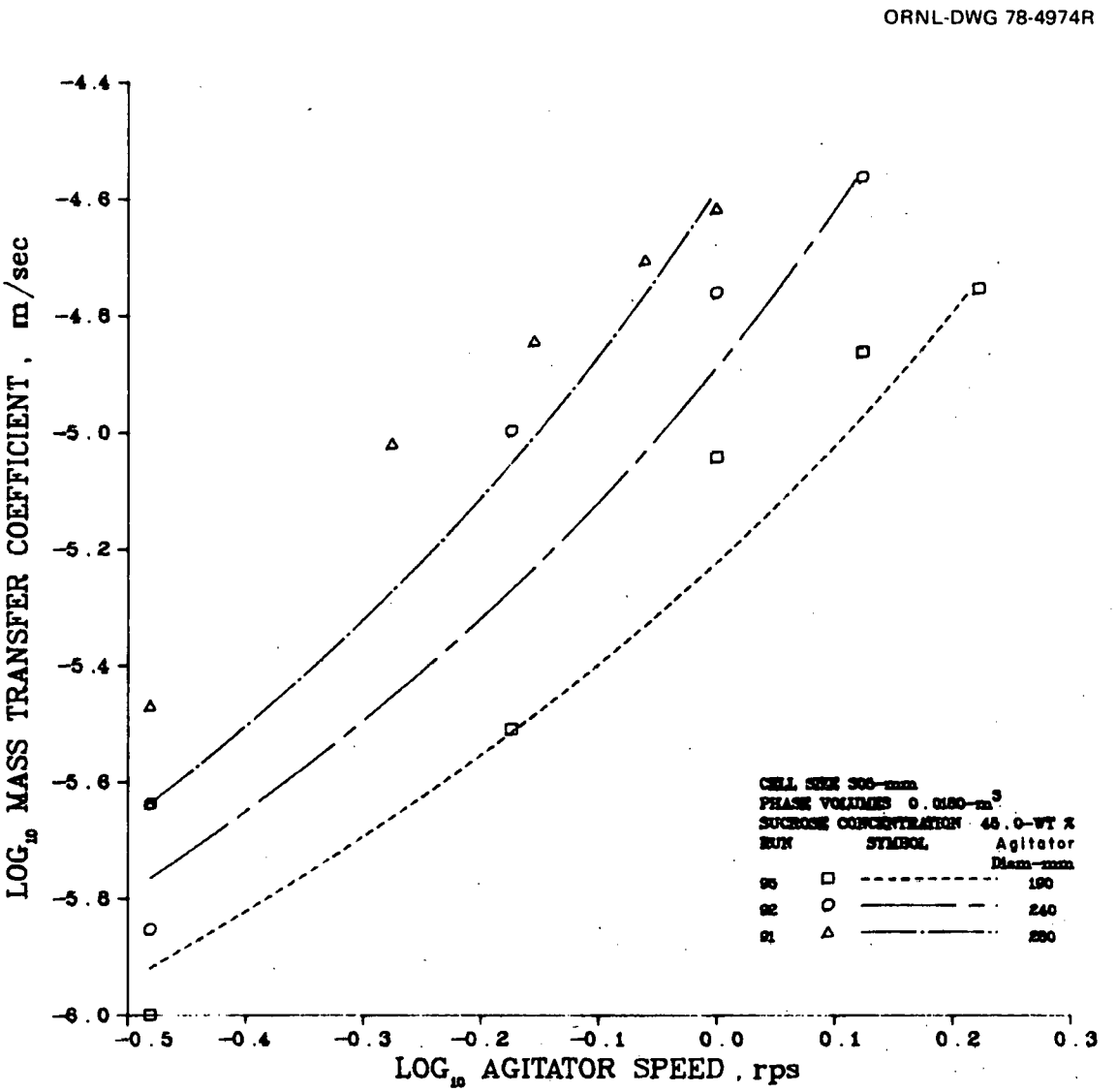

Figure 23. Mass Transfer Coefficient Versus Agitator Speed for Runs 95, 92, and 91.

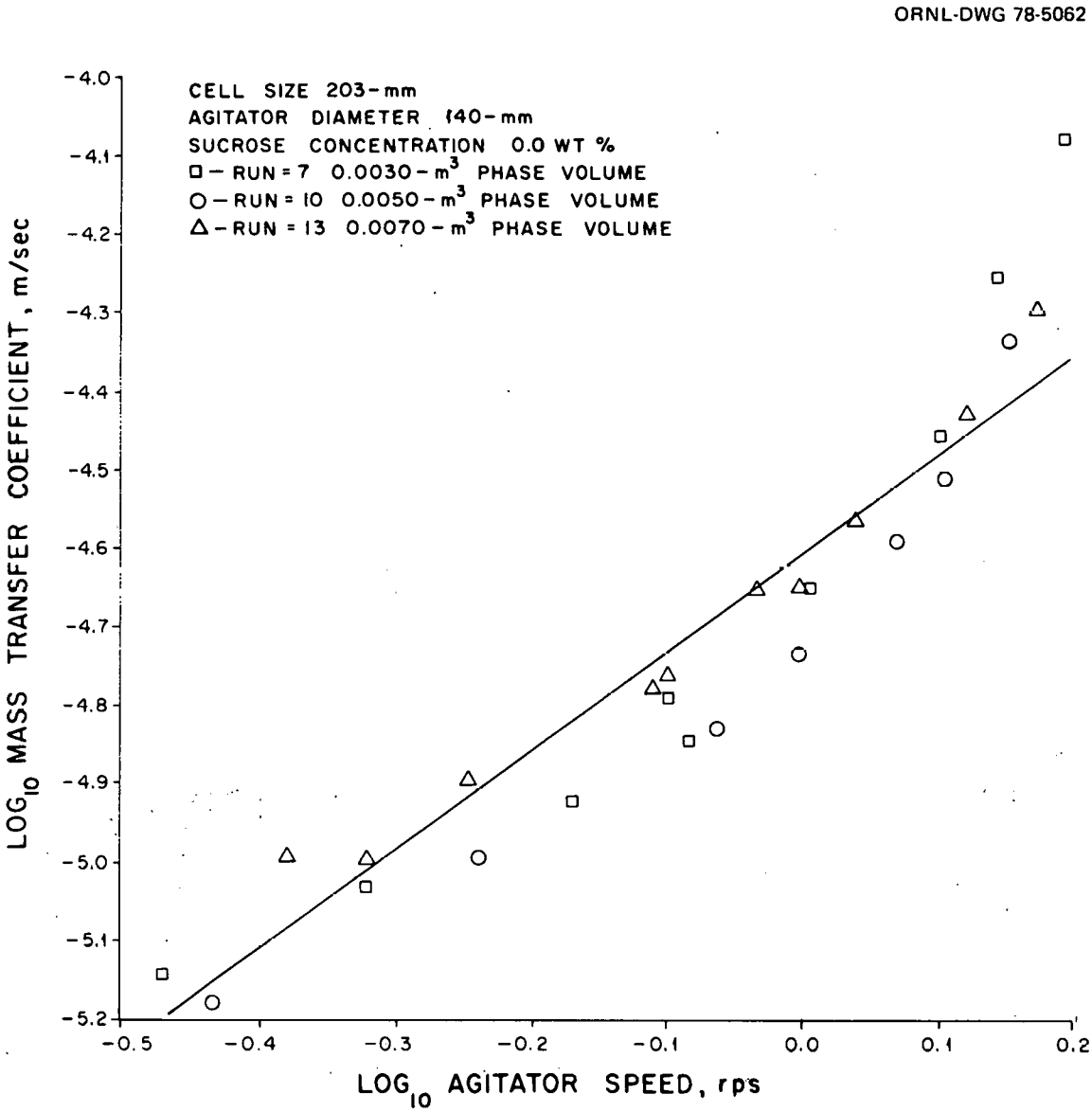

Figure 24. Mass Transfer Coefficient Versus Agitator Speed for Runs 7, 10, and 13.

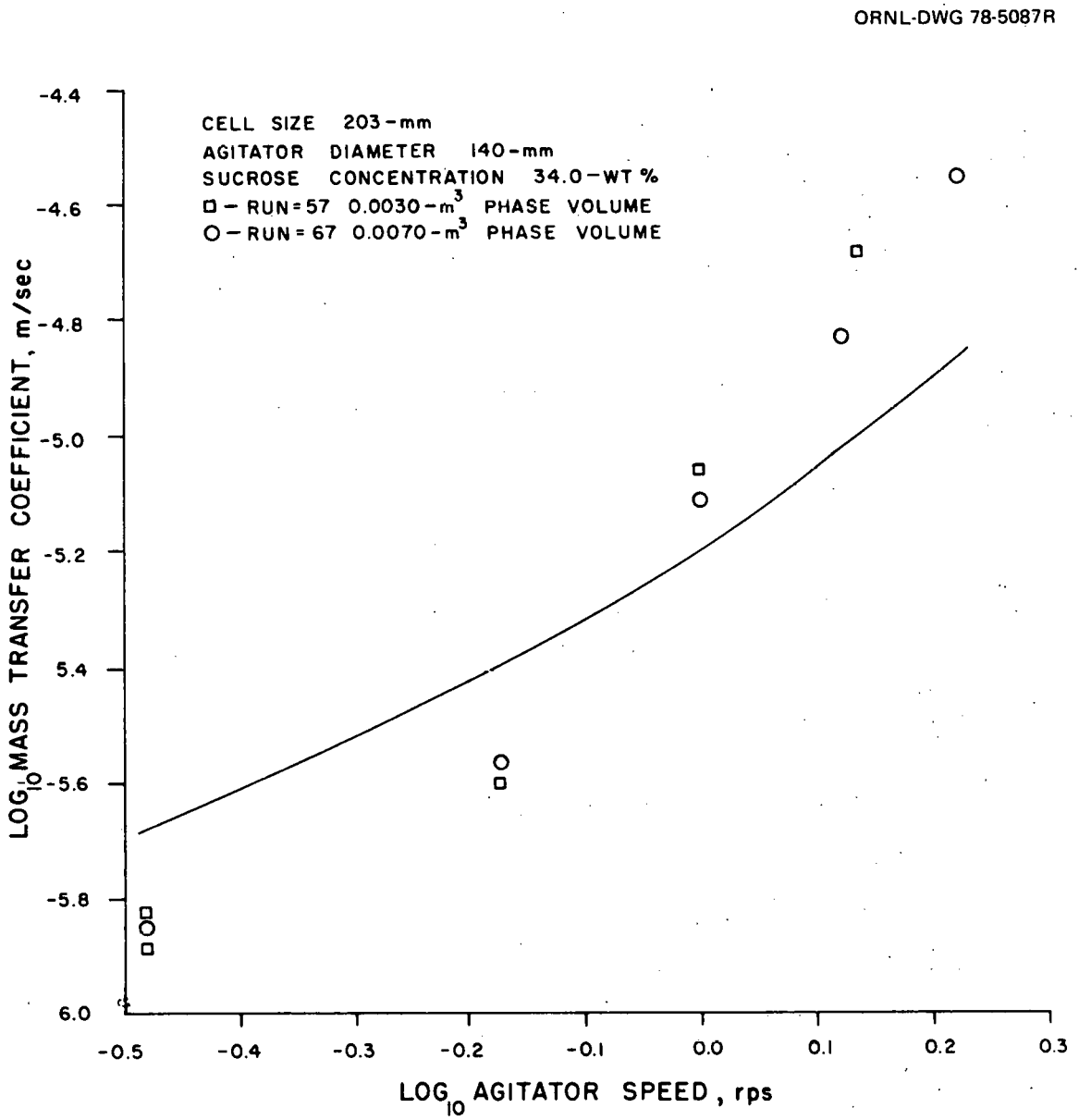

Figure 25. Mass Transfer Coefficient Versus Agitator Speed for Runs 57 and 67.

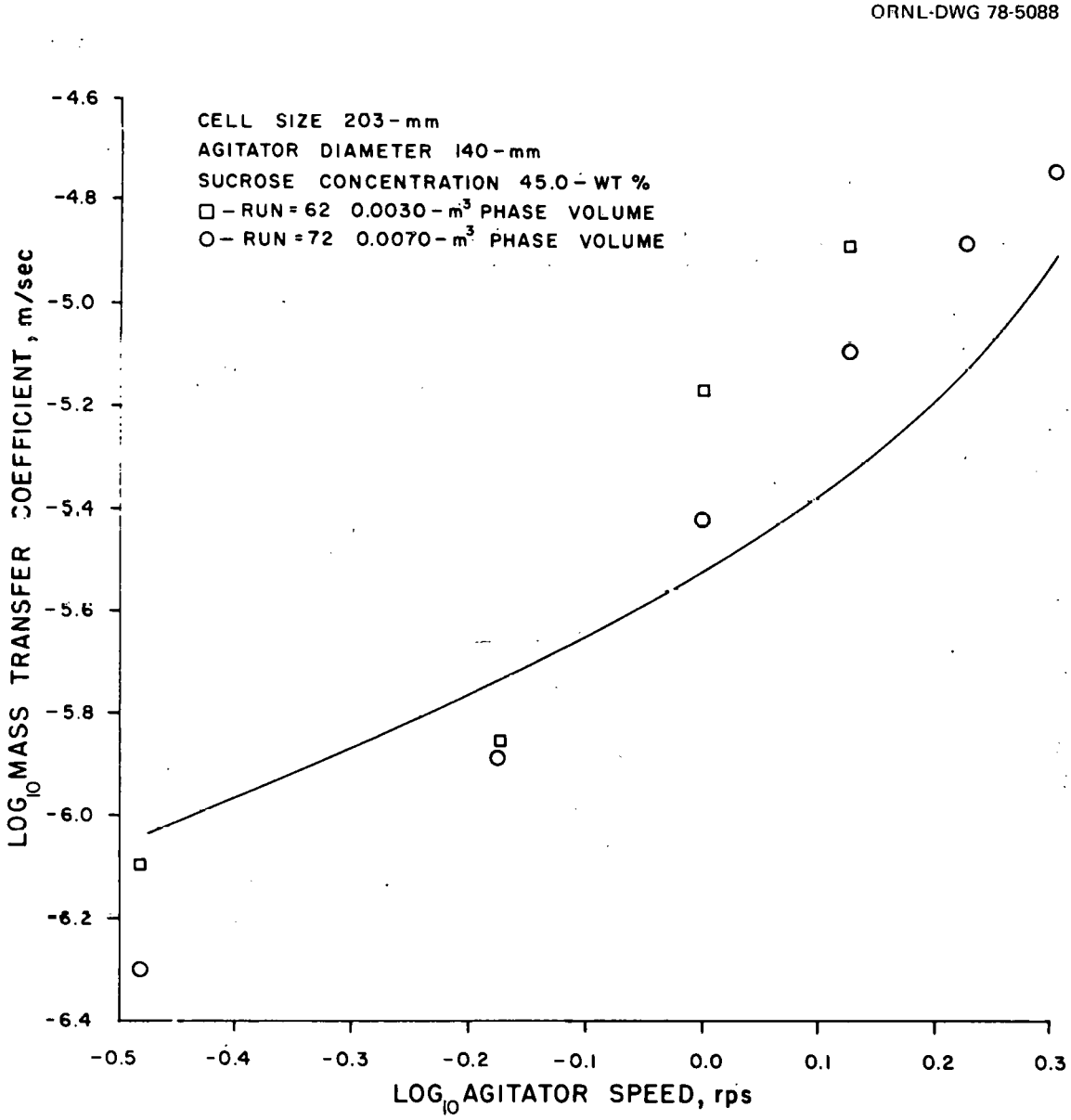

Figure 26. Mass Transfer Coefficient Versus Agitator Speed for Runs 62 and 72.

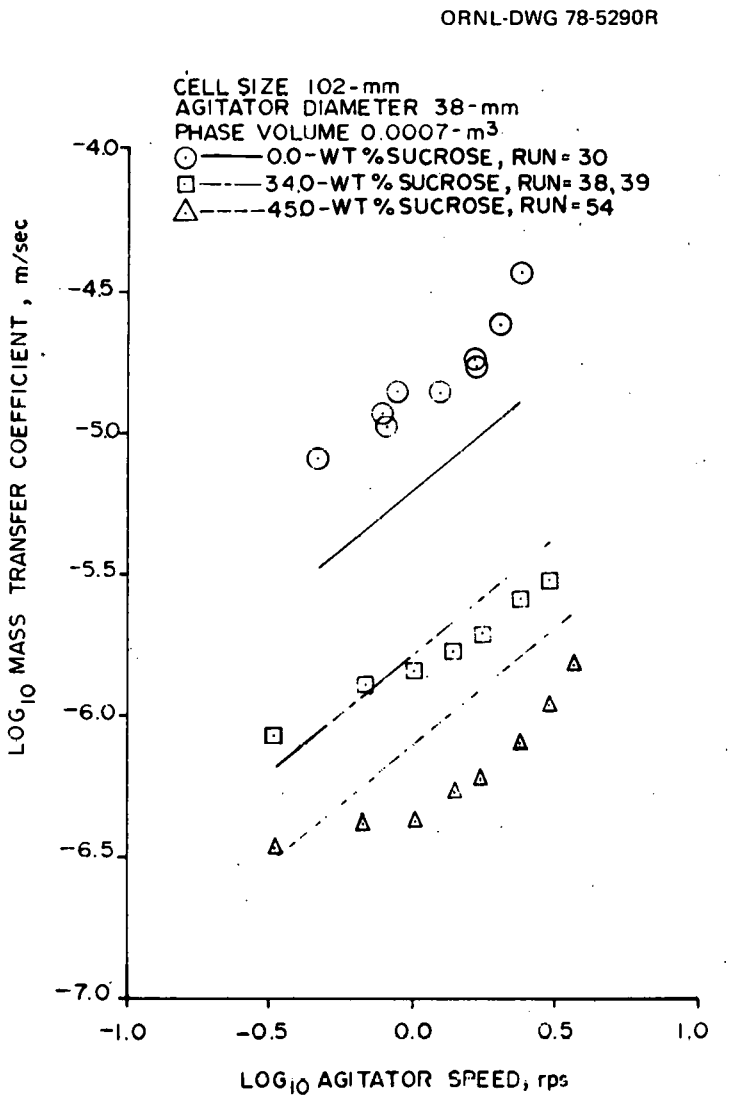

Figure 27. Mass Transfer Coefficient Versus Agitator Speed for Runs 30, 38, 39, and 54.

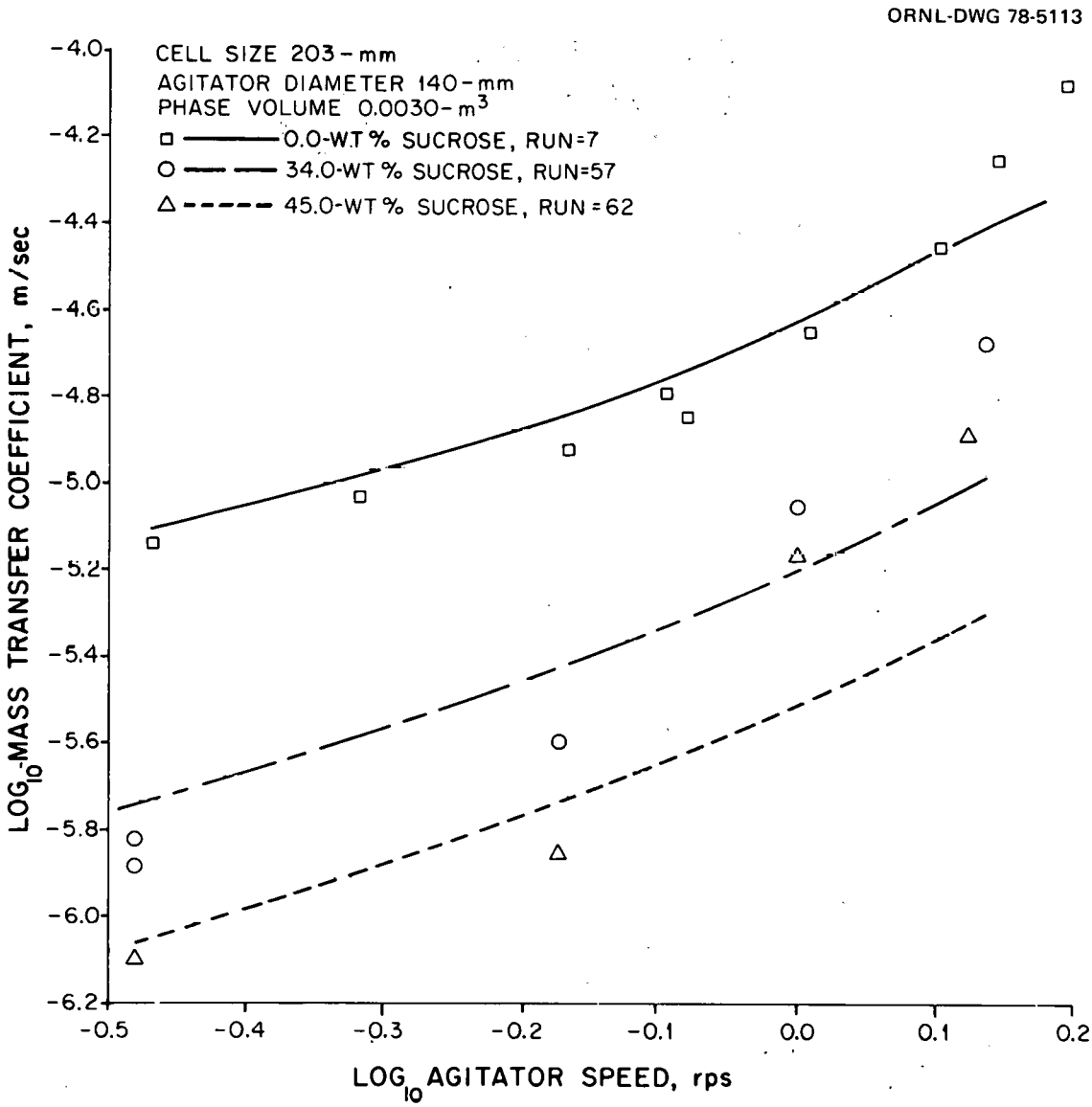

Figure 28. Mass Transfer Coefficient Versus Agitator Speed for Runs 7, 57, and 62.

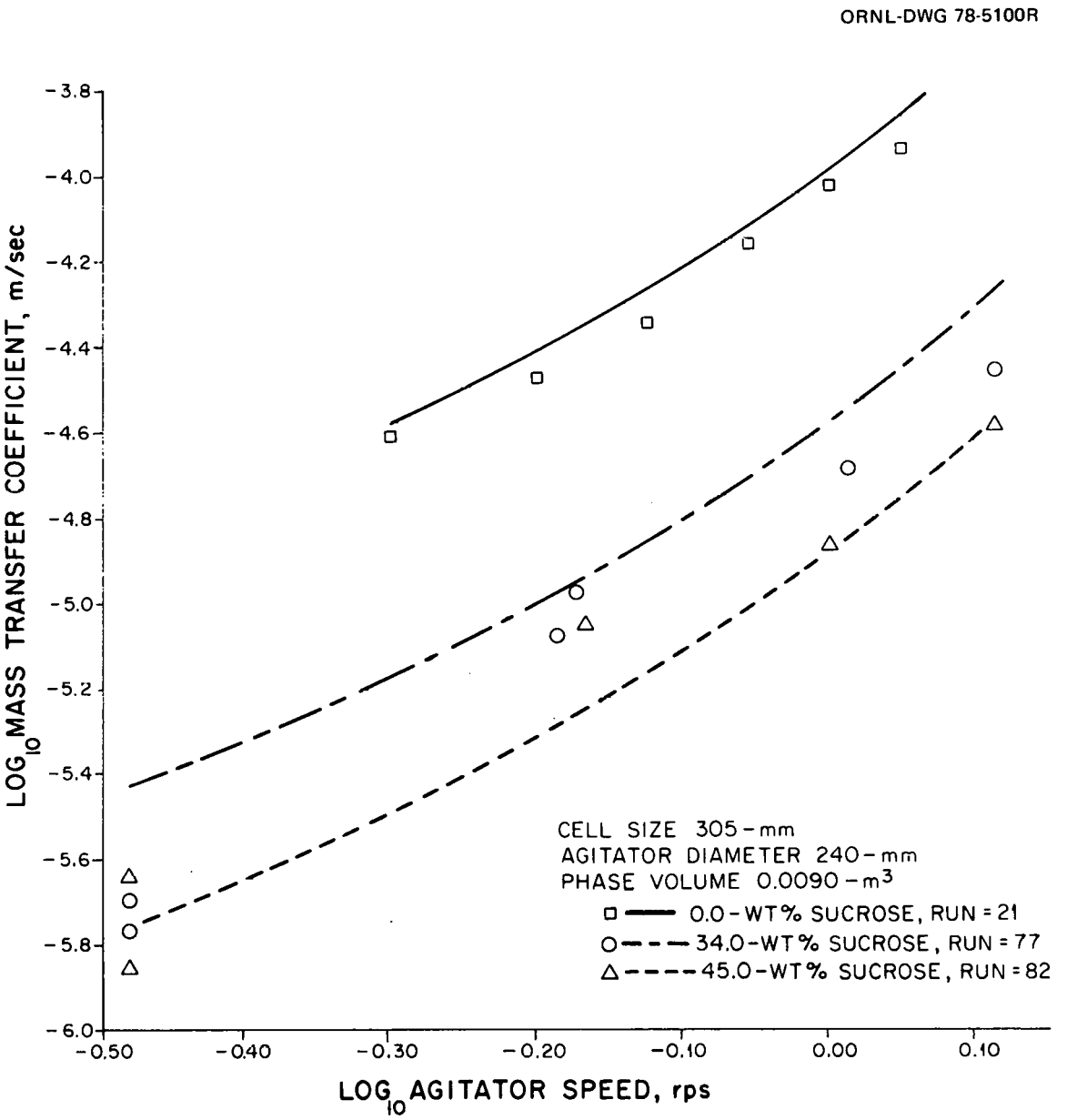

Figure 29. Mass Transfer Coefficient Versus Agitator Speed for Runs 21, 77, and 82.

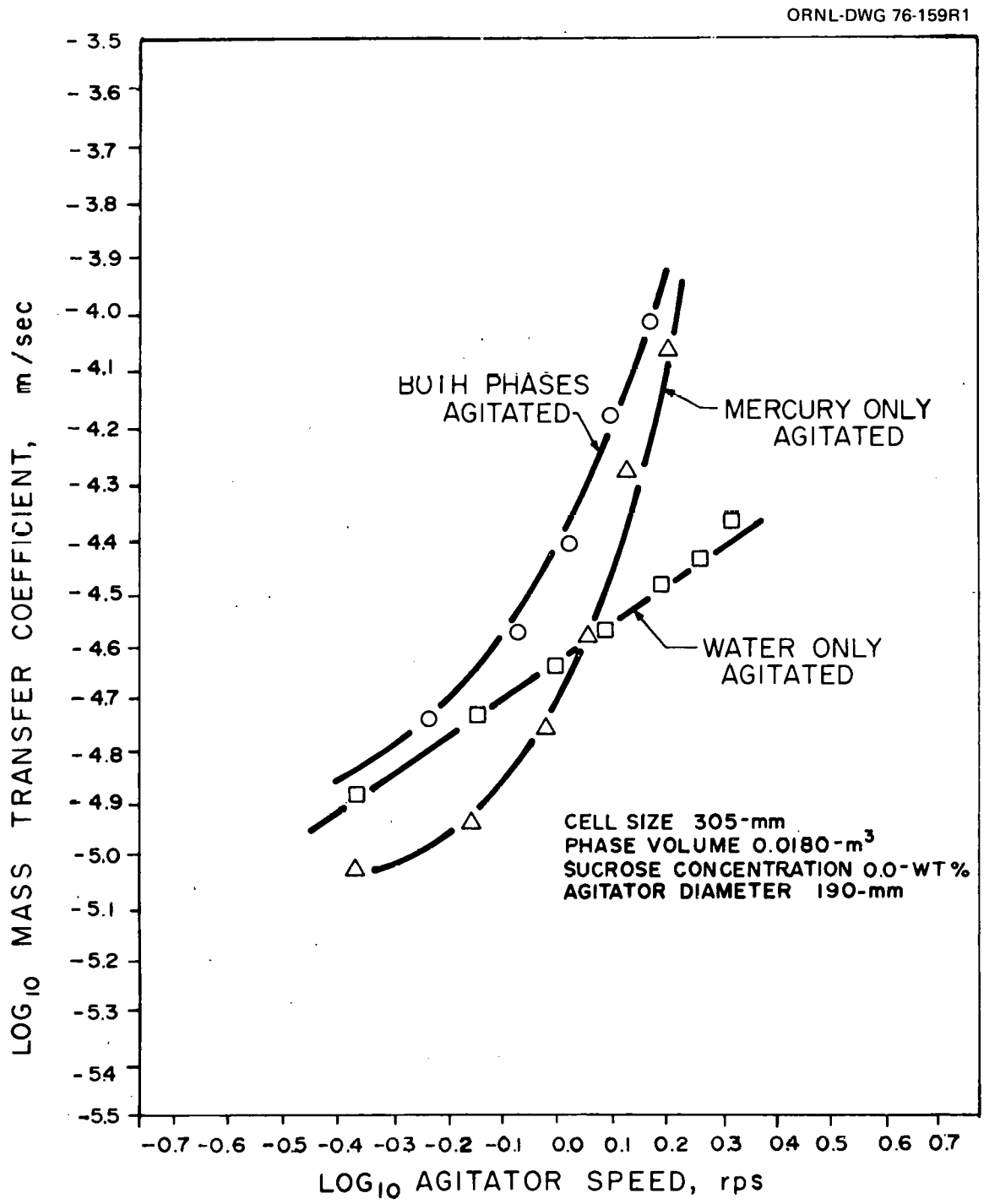

Figure 30. Effect of Selective Phase Agitation on Mass Transfer Coefficient.

The data obtained with an aqueous-phase sucrose concentration of 0.0 wt % are plotted in Figures 5 through 11. Figures 5 and 6 are for the 100-mm cell, Figures 6 through 9 for the 200-mm cell, and Figures 10 and 11 for the 300-mm cell. Each plot gives the measured mass transfer coefficient as a function of the agitator speed on log-log coordinates. One figure is presented for each different phase volume, and separate curves are shown for the various agitator diameters tested.

The data obtained with an aqueous sucrose concentration of 34 wt % are presented in Figures 12 and 13, 14 and 15, and 16 and 17 for the 100-, 200-, and 300-mm cells, respectively. As with the 0.0 wt % sucrose data, a separate figure is given for each phase volume; separate curves are shown for each of the agitator diameters tested.

Figures 18 through 23 summarize the mass transfer data measured with the 45 wt % sucrose electrolyte. The same format is used in these figures as was used with the 0.0 and 34 wt % sucrose data. Figures 18 and 19, 20 and 21, and 22 and 23 are for the 100-, 200-, and 300-mm cells, respectively. One figure is presented for each phase volume tested, and separate curves are included for each agitator diameter tested.

The variation of mass transfer coefficient with agitator speed and phase volume is shown in Figures 24 through 26. These data were measured in the 200-mm cell with the 140-mm-diam agitator. Figure 24 presents the data measured with an aqueous-phase sucrose concentration of 0.0 wt %. Figures 25 and 26 show the data measured with aqueous-phase sucrose concentrations of 34 and 45 wt %, respectively.

The measured mass transfer coefficients are plotted as a function of agitator speed and aqueous-phase sucrose concentration in Figures 27 through 29. Figure 27 is for the 100-mm cell with a phase volume of 0.0007 m^3 and the 38-mm-diam agitator. One curve is shown for each sucrose concentration (0.0, 34, and 45 wt % sucrose). Figure 28 shows data measured in the 200-mm cell with a phase volume of 0.0030 m^3 and the 140-mm-diam agitator; a separate curve is presented for each sucrose concentration. Data measured in the 300-mm cell with a 0.0090-m^3 phase volume, 240-mm-diam agitators, and sucrose concentrations of 0.0, 34, and 45 wt % sucrose are plotted in Figure 29.

The data given in Figure 30 show the relative effect of agitation in each phase on the mass transfer coefficient as compared with simultaneous agitation of both phases. These data were measured in the 300-mm cell with 190-mm-diam agitators and 0.018-m^3 phase volumes.

A complete tabulation of the data obtained in this study is included in Appendix A.

Quinone Diffusion Coefficient

The diffusion coefficient of quinone through the aqueous electrolyte solution was measured as a function of the aqueous-phase sucrose concentration using the d.m.e. apparatus discussed in Chapter IV. The results of these measurements are listed in Table 2. The data that were obtained with the d.m.e. apparatus and were used to calculate the diffusion coefficients listed in Table 2 are tabulated in Appendix B.

Table 2. Quinone Diffusion Coefficient Measured as a Function of Aqueous-Phase Sucrose Concentration

Aqueous Sucrose Concentration (wt %)	Quinone Diffusion Coefficient ($mm^2/sec \times 10^4$)
0.0	6.7
34.0	1.1
45.0	0.46

Physical Properties of the Electrolyte Solution

The physical properties of the electrolyte solution necessary to perform the diffusion coefficient calculations and the correlation of the mass transfer data were measured concurrent with the diffusion coefficient. Both the viscosity and the density of the electrolyte were determined as a function of sucrose concentration. The viscosity was measured with a Brookfield Viscometer, while the density was measured with a standard glass laboratory hydrometer. The results of these measurements and the calculated aqueous-phase Schmidt numbers are listed in Table 3.

Table 3. Physical Properties of the Electrolyte Solution

Sucrose Concentration (wt %)	Solution Viscosity (cP)	Solution Density (g/cm^3)	Aqueous Schmidt Number
0.0	1.17	1.02	1,710
34.0	4.67	1.16	36,600
45.0	10.9	1.22	194,000

CHAPTER VI

DISCUSSION OF EXPERIMENTAL DATA

Effects of Agitator Speed and Agitator Diameter on the Mass Transfer Coefficient

The effects of the agitator speed and agitator diameter on the mass transfer coefficient are shown in Figures 5 through 23 (pages 23-41). In each figure, the logarithm of the measured mass transfer coefficient is plotted versus the logarithm of the agitator speed for constant values of cell size, phase volume, and sucrose concentration. A separate curve is presented for each agitator diameter tested. As shown in Figures 5 through 23, the mass transfer coefficient increased significantly with increasing agitator diameter at a fixed agitator speed. It is also apparent that the increase in mass transfer coefficient with increasing agitator diameter ($\partial k/\partial d$) increases as the agitator speed is raised. For a constant diameter, the curve of mass transfer coefficient versus agitator speed is nonlinear for small agitators but tends to approach linearity with increasing agitator diameter. For the small agitators, this curve appears to be linear in the low agitator speed range but abruptly changes slope at a given agitator speed. The agitator speed at which the slope changes decreases with increasing agitator diameter. Olander and Benedict (9) reported the same slope transition while investigating aqueous-organic systems and attributes it to a change of flow regime at the liquid-liquid interface. Furthermore, the change in flow regime is not necessarily accompanied by marked visual rippling of the liquid-liquid interface (which one would qualitatively associate with interfacial turbulence).

Effect of Phase Volume on the Mass Transfer Coefficient

The effect of phase volume on the measured mass transfer coefficient is shown in Figures 24 through 26 (pages 42-44) for the 203-mm cell. These results are similar to those obtained with the 102- and 305-mm cells.

The sucrose concentrations for the data shown in Figures 24, 25, and 26 are 0.0, 34.0, and 45.0 wt %, respectively. The agitator diameter is 140 mm in each case; the phase volumes range from 0.003 to 0.007 m^3. As shown in the three figures, the effect of changing the phase volume on the measured mass transfer coefficient is slight. Only with a sucrose concentration of 45.0 wt % was any change in mass transfer coefficient detected with increased phase volume (see Figure 26, page 44). The mass transfer coefficients measured with the phase volume of 0.003 m^3 are slightly greater than those measured with a 0.007-m^3 phase volume. This effect can be explained by the greater energy dissipation per unit volume when smaller phase volumes and highest viscosities are used.

Effect of Aqueous-Phase Viscosity on the Mass Transfer Coefficient

The data plotted in Figures 27, 28, and 29 (pages 45-47) for the 102-, 203-, and 305-mm cells, respectively, show the effect of the aqueous-phase viscosity on the measured mass transfer coefficient. Data from runs made with the three aqueous-phase sucrose concentrations, 0.0, 34.0, and 45.0 wt %, are plotted in each figure. The agitator diameter and phase volume were held constant during each set of three runs. Increasing the sucrose concentration, or viscosity, had a dramatic effect on the

mass transfer coefficient; for example, increasing the viscosity by a factor of 10 decreased the mass transfer coefficient by a factor of approximately 35, as shown in Figure 27 (page 45).

The transition (mentioned previously) that results in a change in slope is very apparent for the three viscosities shown in Figure 27 for the 102-mm cell with 38-mm-diam agitators; however, with increased cell size and agitator diameter (Figures 28 and 29, pages 46 and 47), the slope change becomes more gradual and finally disappears altogether for the 305-mm cell with 240-mm-diam agitators.

Effect of Selective Phase Agitation on the Mass Transfer Coefficient

One of the most interesting tests performed in this study was the determination of the relative effect of agitation in each phase on the measured mass transfer coefficient in the aqueous phase.

The 305-mm cell was used with 190-mm-diam agitators and 0.018-m^3 phase volumes. First, the mass transfer coefficient was measured as a function of agitator speed with an agitator in the mercury phase only and in the water phase only. Next, a test was performed with agitators positioned in both phases. The results from these tests, shown in Figure 30 (page 48), indicate that the mass transfer coefficient is most affected by agitation in the water phase when the agitator speed is low. However, as the agitator speed increases, agitation in the mercury begins to affect the (water-side) mass transfer coefficient more strongly than agitation in the water phase alone. Moreover, the mass transfer coefficient resulting from agitation in both phases is not a simple additive function of the mass transfer coefficients resulting from

agitation in one phase only. It is also apparent that the mass transfer coefficient resulting from agitation in the water phase alone is a linear function of the agitator speed in logarithmic coordinates, but the mass transfer coefficient measured for agitation in the mercury phase alone is not a simple, linear logarithmic function of the agitator speed. The results, shown in Figure 30 (page 48), help to provide a qualitative explanation of the shape of the curves shown in Figures 5 through 29 (pages 23-47); they also aid in formulating an equation to correlate all of the mass transfer coefficient data measured.

Comparison of Mass Transfer Coefficient Data with Literature Values

To add credence to the mass transfer data obtained in this study, a comparison was made between the experimental results for the aqueous-mercury system and literature values reported for aqueous-organic systems.

Olander and Benedict (9) reported mass transfer coefficients measured in a 152-mm-diam unbaffled cylindrical cell with 0.001-m^3 phase volumes and 76-mm-diam stirrer bars. The systems used in their study included transfer of isobutanol through water, transfer of water through 30 wt % TBP in hexane, and transfer of water through isobutanol. Unlike the present study, Olander and Benedict used a transient method in which one phase was soluble and physically transferred to the other.

The experimental conditions in this study most closely approximating those of Olander and Benedict are tests made in the 102-mm cell using 0.0007-m^3 phase volumes, 89-mm-diam agitators, and no sucrose.

Figure 31 shows a comparison of the water-mercury data with the aqueous-organic data. In this figure, the results for the aqueous-organic systems bracket those for the water-mercury system. As noted previously, Olander and Benedict also reported the change in slope of the logarithm of the mass transfer coefficient versus the logarithm of the agitator speed.

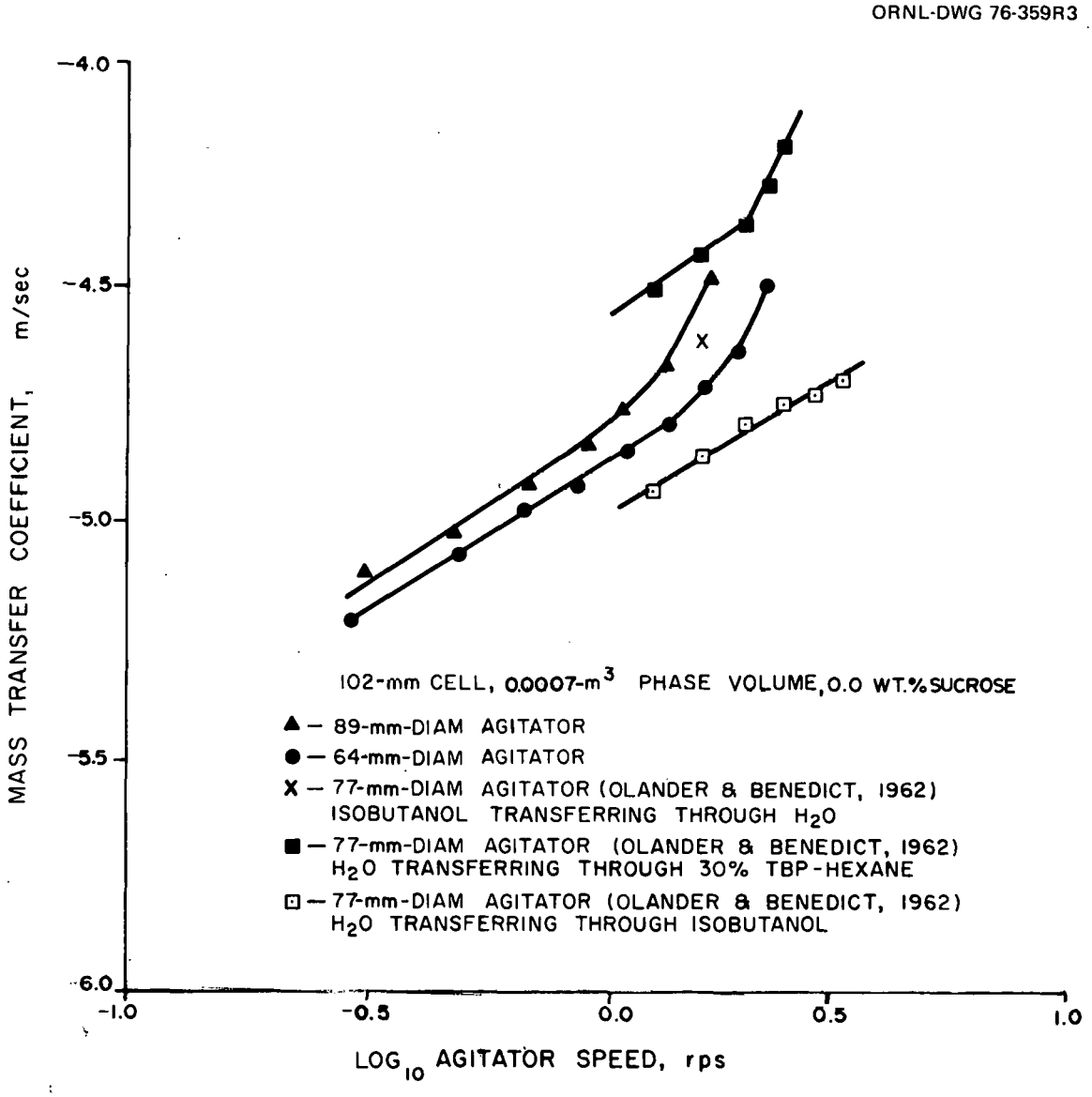

Figure 31. Comparison of Aqueous-Mercury Mass Transfer Data with Aqueous-Organic Mass Transfer Data.

CHAPTER VII

CORRELATION OF DATA

Mass Transfer Data

The mass transfer data were found to be correlated well by the equation

$$N_{Sh} = \left[0.029 \exp(3.3 \times 10^{-6} N_{Re_M})\right] N_{Re_W}^{0.81} N_{Sc_W}^{0.52}, \qquad (18)$$

where the Sherwood number, N_{Sh}, which represents the ratio of convective to molecular mass transfer resistance, is given as a function of the Reynolds number, N_{Re}, based on both the aqueous and mercury phases and the Schmidt number, N_{Sc}, based on aqueous-phase properties.

The numerical coefficients in Equation (18) were calculated from the experimental data reported in Figures 5 through 23 (pages 23-41) along with the physical and transport properties of the aqueous phase given in Tables 2 and 3 (page 51). The IBM 370/91 computer was used with the statistical analysis program SAS (19) to fit the data and to evaluate statistically the degree of fit of Equation (18) to the data. Figure 32 is a parity plot of the experimentally determined Sherwood number versus the Sherwood number calculated from Equation (18). The correlation coefficient for Equation (18) is 0.98, which is defined as (20):

$$\text{Correlation coefficient} = \frac{\sum_{j=1}^{p} \beta_j \left(\sum_{i=1}^{n} (x_{ji} - \bar{x}_j)(y_i - \bar{y}) \right)}{\sum_{i=1}^{n} (y_i - \hat{y}_i)^2 + \sum_{j=1}^{p} \beta_j \left(\sum_{i=1}^{n} (x_{ji} - \bar{x}_j)(y_i - \bar{y}) \right)}, \qquad (19)$$

ORNL-DWG 78-215R2

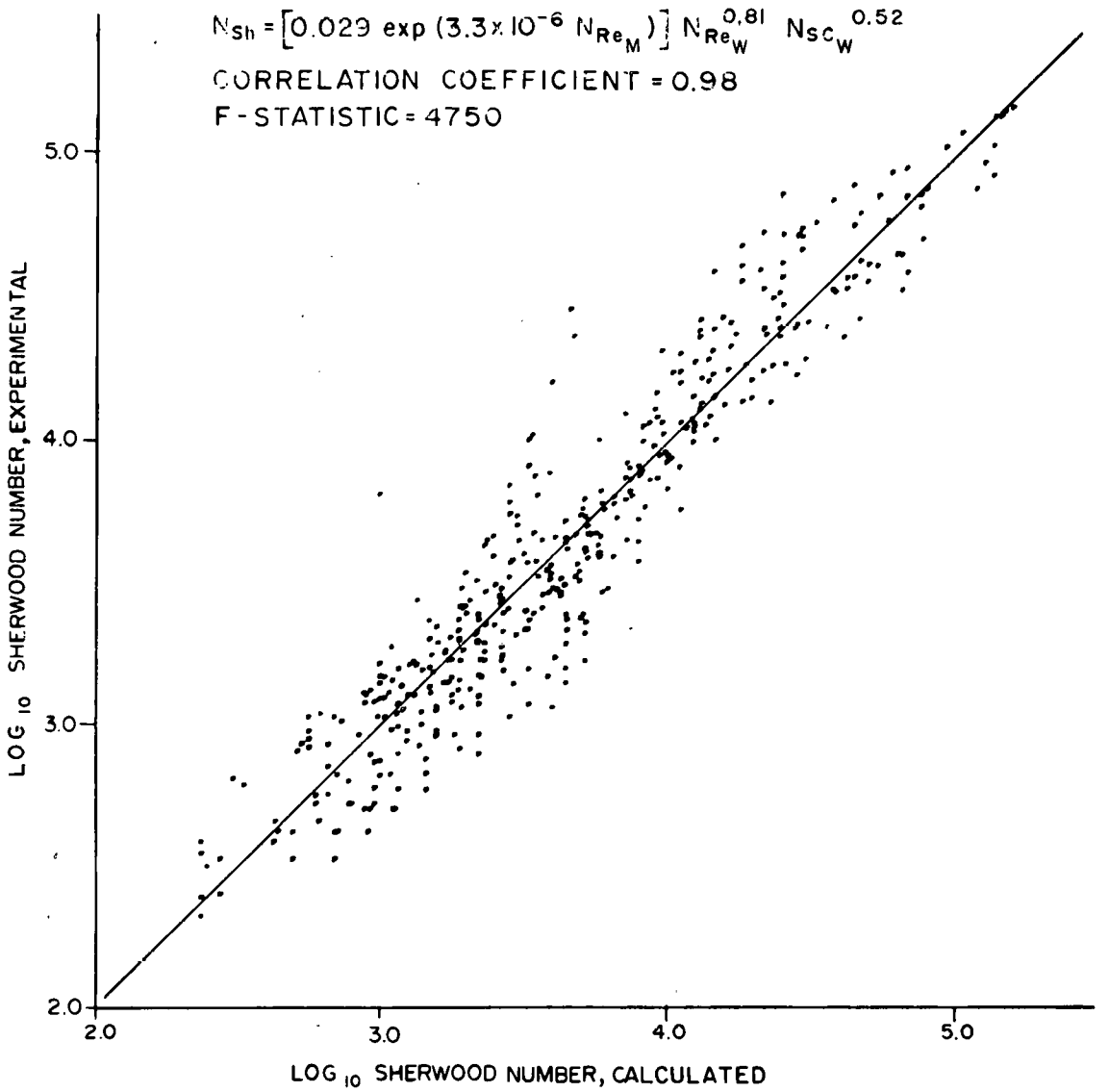

Figure 32. Experimental Sherwood Number Versus Calculated Sherwood Number.

where

y = dependent variable,

x = independent variable,

β = least-squares estimator,

p = number of estimators,

n = number of data points, and

superscripts $-$ and $\hat{}$ refer to mean value and predicted value, respectively. The correlation coefficient estimates the fraction of variation in the data that is accounted for by the correlation. A perfect correlation would have a coefficient of 1.0. The F-statistic for Equation (18) has a value of 4750 and is defined as follows (20):

$$\text{F-statistic} = \frac{\sum_{i=1}^{n} (y_i - \bar{y}_i)^2/(p-1)}{\sum_{i=1}^{n} (y_i - \hat{y}_i)^2/(n-p)} \quad . \tag{20}$$

This statistic takes into account not only the mean-squared deviation of the data, but also the spread or range of the data and the number of parameters in the model equation. The greater the range of the data and the fewer the number of parameters in the model, the higher the value of the F-statistic. A perfect correlation would result in an F-statistic of infinity.

Discussion of Correlation

A total of 15 different correlating equations similar to Equation (18) were tried with various degrees of success. In the development of

Equation (18), one of the objectives was to find the simplest equation which would represent the data accurately. Of the equations tested, the final selection had both the highest correlation coefficient, 0.98, and the highest F-statistic, 4750, with the number of parameters equal to or less than those in the other models. The exponents of the aqueous-phase Reynolds and Schmidt numbers are also found to be quite reasonable, based on both statistical analysis and comparison with similar literature values.

The 95% confidence interval was calculated for each constant in Equation (18), to give:

$$N_{Sh} = \left[\left(0.029\ {}^{+0.068}_{-0.013}\right) \exp\left((3.3 \pm 0.5) \times 10^{-6}\ N_{Re_M}\right)\right] \times \left(N_{Re_w}{}^{0.81 \pm 0.07}\ N_{Sc_w}{}^{0.52 \pm 0.04}\right). \quad (21)$$

The 95% confidence interval results in about a 10% variation in each coefficient other than the intercept term. The intercept term has a relatively large variation due to the wide range over which data were taken. A relatively large change in the intercept term causes only a small change in the slope coefficients. Based on the 95% confidence interval, Equation (18) fits the data quite satisfactorily.

The parity plot given in Figure 32 shows qualitatively how well Equation (18) predicts the experimentally determined values of the Sherwood number. A computer program which calculated the mass transfer coefficient using Equation (18) and appropriate values of the experimental

parameters was prepared to evaluate further the utility of Equation (18) for predicting individual data points. Such comparisons can show trends in the correlation more effectively than parity plots. The results of these calculations are illustrated graphically in Figures 5 through 29 (pages 23-47). All of the curves presented in these figures are calculated from Equation (18).

As expected in correlations of this type, Equation (18) does not fit every set of data perfectly; however, it does predict the general data trends. In none of the cases studied did the calculated curves vary from the data by more than 40% (see run 75 in Figure 21, page 39).

The terms in Equation (18) were arrived at by observing the data trends as a function of operating parameters, studying the types of correlations used previously for stirred contactors, and intuitive reasoning. Of the several tested, the combination of dimensionless groups that worked best is described below. The intercept term [shown in brackets in Equation (18)] was arrived at by inspection of Figure 30 (see page 48). The mass transfer coefficient measured when only the mercury was agitated appeared to be an exponential function of the agitator speed. The dimensionless group that contains the agitator speed is the Reynolds number based on agitator tip velocity. Similarly, by inspection of Figure 30 (page 48), when only the aqueous phase was agitated, the mass transfer coefficient is a linear function of the agitator speed. Again, the Reynolds number was used, this time based on the aqueous-phase properties. Finally, the importance of the Schmidt number was suggested by work performed by several researchers (7, 8, 9,

10, 12, 15) who determined that, in turbulent systems, the mass transfer coefficient is a linear function of the Schmidt number.

McManamey et al. (12) determined conclusively that the Schmidt number dependence of the Sherwood number was 0.5 by measuring the transfer rates of helium and toluene and of helium and butanol through water. The aqueous Reynolds number exponent of 0.81 is typical of forced convection mass transfer and is quite close to the exponent of 0.75 reported by Bulicka and Prochazka (15).

Equation (9) developed by Bulicka and Prochazka (15) is similar to Equation (18) developed in this study. The only significant difference between them lies in the intercept term. A parity plot (Figure 33) of the experimental Sherwood number versus the Sherwood number predicted by Equation (9) was prepared to test Equation (9) with the aqueous-mercury data. Equation (9) overpredicts the Sherwood number between values of 100 and 4,000 and underpredicts it between values of 4,000 and 160,000. It is important to note that the data measured in this study cover a range of Sherwood numbers from about 100 to about 160,000. Equation (9) was determined for data with Sherwood numbers ranging from only 500 to 3,000. One, therefore, would not necessarily expect it to provide an accurate prediction of the Sherwood number far outside the range of data from which it was developed.

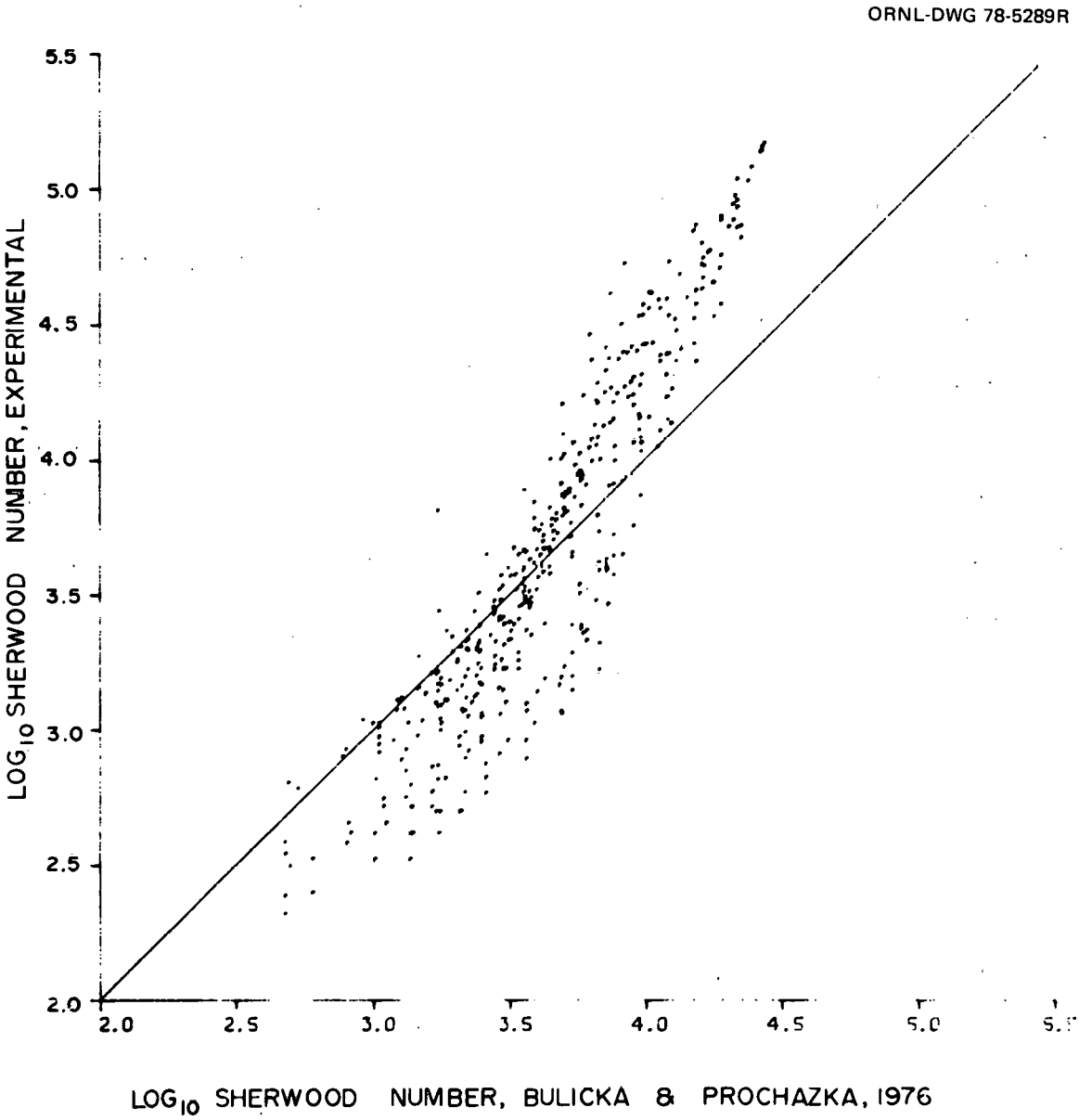

Figure 33. Experimental Sherwood Number Versus Sherwood Number Calculated by Bulicka and Prochazka.

CHAPTER VIII

CONCLUSIONS AND RECOMMENDATIONS

Conclusions

The original objectives of the thesis were fulfilled: (a) to measure polarographically the mass transfer rates of an electrolyte through an aqueous film in agitated, two-phase, nondispersing liquid-liquid contactors, using an aqueous electrolyte solution as the light phase and mercury as the heavy phase; and (b) to correlate the mass transfer data obtained in (a). The evidence supporting these objectives is given in Chapters V, VI, and VII.

Specific conclusions which can be drawn from this work are:

1. The aqueous-film mass transfer coefficients measured in this study can be correlated well by a new and improved correlation containing Reynolds numbers based on each phase and the Schmidt number based on the aqueous phase [see Equation (18) and Figure 32, page 59].
2. Of those investigated, the parameters affecting the mass transfer coefficient most significantly are the agitator speed, agitator diameter, and aqueous-phase viscosity.
3. The phase volume has very little effect on the mass transfer coefficient, within the range of conditions examined.
4. The correlation developed in this study is similar to that developed by Bulicka and Prochazka (15), but data were measured over a much wider range of Sherwood numbers and therefore produced a significantly better correlation.

Recommendations

For further expansion of this study, the following recommendations can be made:

1. Develop a method for measuring the mass transfer coefficient on the mercury side of the aqueous-mercury interface.
2. Develop an apparatus to vary independently the agitator speed in each phase, thereby allowing further elucidation of the effect of agitation in one phase on mass transfer in each phase.
3. Study bubble-induced mass transfer where bubbles of gas would introduce turbulence instead of turbines, thus eliminating the need for a mechanically driven agitator.

LIST OF REFERENCES

LIST OF REFERENCES

1. M. W. Rosenthal et al., The Development Status of Molten-Salt Breeder Reactors, Sec. II, ORNL-4812 (August 1972).

2. S. D. Clinton, Oak Ridge National Laboratory, personal communication, 1976.

3. V. A. Maroni, R. D. Walson, and G. E. Staahl, "Some Preliminary Considerations of a Molten-Salt Extraction Process to Remove Tritium from Liquid Lithium Fusion Reactor Blankets," Nucl. Technol. 25, 83-91 (1975).

4. J. S. Watson, Oak Ridge National Laboratory, personal communication, 1976.

5. J. B. Lewis, "The Mechanism of Mass Transfer of Solutes Across Liquid-Liquid Interfaces," Chem. Eng. Sci. 3, 248 (1954).

6. K. F. Gordon and T. K. Sherwood, "Mass Transfer Between Two Liquid Phases," Chem. Eng. Prog., Symp. Ser. 50(10), 15 (1954).

7. W. J. McManamey, "Molecular Diffusion and Liquid-Liquid Mass Transfer in Stirred Cells," Chem. Eng. Sci. 15, 251 (1961).

8. G. R. A. Mayers, "The Correlation of Individual Film Coefficients of Mass Transfer in a Stirred Cell," Chem. Eng. Sci. 16, 69 (1961).

9. D. R. Olander and M. Benedict, "The Mechanism of Extraction by Tributyl Phosphate-n-Hexanol Solvents," Nucl. Sci. Eng. 14, 287 (1962).

10. D. R. Olander, "A Modified Model of Stirred Vessel Mass Transfer," Chem. Eng. Sci. 19, 275 (1964).

11. M. J. Loosemore and A. P. Prosser, "Mass Transfer in a Stirred Vessel Extractor," Chem. Eng. Sci. 18, 555 (1963).

12. W. M. McManamey, J. T. Davies, J. M. Woolen, and J. R. Coe, "The Influence of Molecular Diffusion on Mass Transfer Between Turbulent Liquids," Chem. Eng. Sci. 28, 1061 (1973).

13. J. T. Davies, Turbulence Phenomena, Academic Press, New York, 1972.

14. W. J. McManamey, S. K. S. Multani, and J. T. Davies, "Molecular Diffusion and Liquid-Liquid Mass Transfer in Stirred Transfer Cells," Chem. Eng. Sci. 30, 1536 (1975).

15. J. Bulicka and J. Prochazka, "Mass Transfer Between Two Turbulent Liquid Phases," Chem. Eng. Sci. 31, 137 (1976).

16. J. S. Watson, "A Study of Detached Turbulence Promoters for Increasing Mass Transfer Rates in Aqueous Chemical Flow," Ph.D. Dissertation, University of Tennessee (1967).

17. I. M. Kolthoff and J. J. Lingane, Polarography, p. 186, Interscience, New York, 1946.

18. I. M. Kolthoff and J. J. Lingane, Polarography, p. 45, Interscience, New York, 1952.

19. A. J. Barr et al., A User's Guide to SAS 76, Sparks Press, Raleigh, N.C., 1976.

20. R. E. Walpole and R. H. Myers, Probability and Statistics for Engineers and Scientists, p. 321, Macmillan, New York, 1972.

THIS PAGE

WAS INTENTIONALLY

LEFT BLANK

APPENDIXES

APPENDIX A

RUN CONDITIONS FOR AND RESULTS FROM MASS TRANSFER COEFFICIENT MEASUREMENTS

A listing of the experimental variables tested with aqueous sucrose concentrations of 0.0, 34.0, and 45.0 wt % is given in Tables 4, 5, and 6, respectively. Each table contains the cell size, phase volume, agitator diameter, and quinone concentration for the individual runs. Following the quinone concentration is a tabulation of agitator speed, measured diffusion current, and calculated mass transfer coefficient.

All of the original experimental data are recorded in unclassified notebooks numbered A-7551-G (pages 1-92), A-7639, and A-7640-G, which are the property of the Oak Ridge National Laboratory.

Table 4. Experimental Conditions and Results Measured with 0.0 wt % Sucrose in the Aqueous Phase

Run	Cell Size ($m \times 10^3$)	Phase Volume ($m^3 \times 10^3$)	Agitator Diameter ($m \times 10^3$)	Quinone Concentration (kg-mole/m^3)	Agitator Speed (rps)	Diffusion Current ($A \times 10^3$)	Mass Transfer Coefficient (m/sec $\times 10^3$)
6	203.0	3.0	190.0	0.0010	.40	92.5	.0116
					.63	169.0	.0211
					.82	255.0	.0320
					1.00	271.0	.0681
					1.10	366.0	.0918
					1.15	290.0	.1450
					1.35	372.0	.1870
7	203.0	3.0	140.0	0.0010	.34	57.6	.0072
					.48	74.2	.0093
					.68	94.7	.0119
					.83	114.0	.0142
					.80	128.0	.0161
					1.02	178.0	.0223
					1.27	277.0	.0348
					1.40	440.0	.0552
					1.57	660.0	.0829
8	203.0	3.0	89.0	0.0010	.53	62.9	.0079
					.73	75.1	.0094
					1.05	99.5	.0125
					1.20	116.0	.0145
					1.42	164.0	.0206
					1.67	149.0	.0187
					1.97	193.0	.0242
					2.47	298.0	.0374
9	203.0	5.0	89.0	0.005	.37	19.5	.0049
					.50	23.0	.0058
					.60	28.2	.0071
					.77	32.6	.0082

Table 4 (Continued)

Run	Cell Size ($m \times 10^3$)	Phase Volume ($m^3 \times 10^3$)	Agitator Diameter ($m \times 10^3$)	Quinone Concentration (kg-mole/m^3)	Agitator Speed (rps)	Diffusion Current ($A \times 10^3$)	Mass Transfer Coefficient ($m/sec \times 10^3$)
					.77	29.5	.0074
					.98	35.5	.0089
					1.03	39.0	.0098
					1.13	39.5	.0099
					1.20	44.2	.0111
					1.23	43.5	.0109
					1.42	49.9	.0125
					1.43	51.8	.0130
					1.67	64.0	.0161
					1.70	64.0	.0161
					1.88	85.1	.0214
					1.95	87.0	.0218
10	203.0	5.0	140.0	0.0005	.37	26.2	.0066
					.58	40.3	.0101
					.87	58.7	.0147
					1.00	73.1	.0183
					1.18	102.0	.0255
					1.28	122.0	.0306
					1.43	183.0	.0458
11	203.0	5.0	190.0	0.0005	.48	57.9	.0145
					.63	88.7	.0223
					.67	86.6	.0217
					.73	109.0	.0274
					.83	125.0	.0313
					.93	167.0	.0419
					.97	189.0	.0475
					1.10	301.0	.0756
12	203.0	7.0	89.0	0.0005	.45	27.2	.0068
					.63	32.2	.0081
					.83	38.3	.0096
					.98	43.3	.0109

Table 4 (Continued)

Run	Cell Size ($m \times 10^3$)	Phase Volume ($m^3 \times 10^3$)	Agitator Diameter ($m \times 10^3$)	Quinone Concentration ($kg\text{-}mole/m^3$)	Agitator Speed (rps)	Diffusion Current ($A \times 10^3$)	Mass Transfer Coefficient ($m/sec \times 10^3$)
					1.22	50.3	.0126
					1.42	55.9	.0140
					1.57	61.4	.0154
					1.72	69.5	.0174
					1.87	76.5	.0192
					2.10	84.6	.0212
					2.10	86.6	.0217
					2.30	98.8	.0248
					2.45	121.0	.0303
13	203.0	7.0	140.0	0.0005	.42	40.6	.0102
					.48	40.3	.0101
					.57	50.8	.0127
					.78	66.0	.0166
					.80	69.0	.0173
					.93	88.3	.0222
					1.00	88.6	.0224
					1.10	109.0	.0272
					1.33	148.0	.0372
					1.50	201.0	.0504
14	203.0	7.0	190.0	0.0005	1.30	443.0	.1120
					1.12	331.0	.0831
					.97	232.0	.0582
					.67	174.0	.0436
					.58	141.0	.0353
					.43	108.0	.0270
					.28	62.1	.0156
15	102.0	0.7	64.0	0.0010	.30	12.5	.0063
					.52	17.5	.0088
					.70	22.0	.0110
					.92	24.5	.0123
					1.17	29.5	.0148

Table 4 (Continued)

Run	Cell Size ($m \times 10^3$)	Phase Volume ($m^3 \times 10^3$)	Agitator Diameter ($m \times 10^3$)	Quinone Concentration ($kg\text{-}mole/m^3$)	Agitator Speed (rps)	Diffusion Current ($A \times 10^3$)	Mass Transfer Coefficient ($m/sec \times 10^3$)
					1.43	33.5	.0168
					1.70	40.0	.0201
					2.00	48.5	.0243
					2.30	66.5	.0334
16	102.0	0.7	89.0	0.0010	.32	16.1	.0081
					.50	19.6	.0098
					.97	30.2	.0151
					1.20	36.2	.0181
					1.42	44.8	.0225
					1.77	70.5	.0354
					.72	24.7	.0124
17	102.0	0.9	64.0	0.0010	.27	13.1	.0066
					.50	16.6	.0083
					.75	21.1	.0106
					1.00	24.7	.0124
					1.27	28.2	.0141
					1.50	32.2	.0161
					1.80	36.9	.0185
					2.00	41.3	.0207
					2.32	50.8	.0255
18	102.0	0.9	89.0	0.0010	.47	19.1	.0096
					.70	24.2	.0121
					1.03	31.7	.0159
					1.40	42.3	.0212
					1.70	55.4	.0278
					1.87	66.5	.0334
19	305.0	9.0	89.0	0.00020	.60	47.3	.0139
					.87	59.4	.0165
					1.13	73.5	.0205
					1.50	88.6	.0247

Table 4 (Continued)

Run	Cell Size ($m \times 10^3$)	Phase Volume ($m^3 \times 10^3$)	Agitator Diameter ($m \times 10^3$)	Quinone Concentration ($kg\text{-}mole/m^3$)	Agitator Speed (rps)	Diffusion Current ($A \times 10^3$)	Mass Transfer Coefficient ($m/sec \times 10^3$)
					1.80	101.0	.0281
					2.03	123.0	.0342
					2.37	147.0	.0410
					2.67	179.0	.0499
21	305.0	9.0	240.0	0.00020	.50	88.8	.0247
					.63	122.0	.0339
					.75	163.0	.0455
					.88	250.0	.0696
					1.00	341.0	.0950
					1.12	415.0	.1160
22	305.0	9.0	280.0	0.00020	.35	61.9	.0173
					.43	84.6	.0236
					.53	118.0	.0328
					.65	147.0	.0408
					.82	312.0	.0869
24	305.0	18.0	89.0	0.0020	.48	33.7	.0094
					.65	36.7	.0102
					.93	48.8	.0136
					1.18	55.8	.0155
					1.35	59.9	.0167
					1.77	65.9	.0184
					2.00	81.1	.0226
					2.33	98.6	.0275
					2.67	123.0	.0344
					3.13	179.0	.0498
25	305.0	18.0	140.0	0.00020	.42	33.3	.0093
					.60	43.4	.0121
					.85	55.5	.0155
					1.07	68.7	.0191
					1.37	100.0	.0279

Table 4 (Continued)

Run	Cell Size ($m \times 10^3$)	Phase Volume ($m^3 \times 10^3$)	Agitator Diameter ($m \times 10^3$)	Quinone Concentration ($kg\text{-}mole/m^3$)	Agitator Speed (rps)	Diffusion Current ($A \times 10^3$)	Mass Transfer Coefficient ($m/sec \times 10^3$)
					1.62	138.0	.0386
					1.82	194.0	.0542
					2.15	317.0	.0884
					2.33	407.0	.1130
26	305.0	18.0	190.0	0.00020	.57	59.4	.0165
					.83	85.6	.0238
					1.03	127.0	.0354
					1.25	223.0	.0621
					1.47	331.0	.0922
					1.67	434.0	.1210
27	305.0	18.0	240.0	0.00020	.33	57.5	.0160
					.53	86.3	.0241
					.67	134.0	.0372
					.85	187.0	.0521
					.98	253.0	.0705
					1.15	413.0	.1150
28	305.0	18.0	280.0	0.00020	.27	51.4	.0143
					.38	71.9	.0200
					.55	121.0	.0338
					.67	166.0	.0464
					.80	230.0	.0642
					.92	335.0	.0934
97	305.0	9.0	190.0	0.00020	.33	48.1	.0130
					.67	92.5	.0260
					1.00	203.5	.0570
					1.33	314.5	.0880
					1.67	473.6	.1320
					.33	48.1	.0130
98	305.0	9.0	140.0	0.00020	.33	40.7	.0110

Table 4 (Continued)

Run	Cell Size ($m \times 10^3$)	Phase Volume ($m^3 \times 10^3$)	Agitator Diameter ($m \times 10^3$)	Quinone Concentration (kg-mole/m^3)	Agitator Speed (rps)	Diffusion Current ($A \times 10^3$)	Mass Transfer Coefficient (m/sec $\times 10^3$)
					.67	66.6	.0190
					1.00	88.0	.0250
					1.33	129.5	.0360
					1.67	188.7	.0530
30	102.0	0.7	38.0	0.0010	.80	23.4	.0117
					1.20	28.5	.0143
					1.57	35.6	.0179
					.47	16.4	.0082
					.80	21.5	.0108
					1.20	27.3	.0137
					1.57	34.8	.0175
					1.57	34.5	.0173
					2.00	46.7	.0243
					2.30	71.1	.0357

Table 5. Experimental Conditions and Results Measured with 34 wt % Sucrose in the Aqueous Phase

Run	Cell Size ($m \times 10^3$)	Phase Volume ($m^3 \times 10^3$)	Agitator Diameter ($m \times 10^3$)	Quinone Concentration ($kg\text{-}mole/m^3$)	Agitator Speed (rps)	Diffusion Current ($A \times 10^3$)	Mass Transfer Coefficient ($m/sec \times 10^3$)
38	102.0	0.7	38.0	0.0005	.33	1.01	.0010
					.68	1.32	.0013
					1.00	1.56	.0016
					1.37	1.76	.0018
					1.73	2.07	.0021
					2.33	2.64	.0027
					3.00	3.30	.0033
					.35	0.86	.0009
					2.33	2.51	.0025
					3.00	3.17	.0032
39	102.0	0.7	38.0	0.0005	.33	0.74	.0007
					.67	1.10	.0011
					1.03	1.31	.0013
					1.40	1.53	.0015
					1.73	1.73	.0017
					2.60	2.41	.0024
					3.00	2.67	.0027
					.33	0.61	.0006
					1.73	1.53	.0015
					3.00	2.63	.0026
40	102.0	0.7	64.0	0.0005	.33	1.76	.0018
					.33	1.52	.0015
					.67	2.51	.0025
					1.00	3.39	.0034
					.33	1.48	.0015
					.70	2.17	.0022
					1.02	2.95	.0030
					1.37	4.14	.0042
					1.70	7.88	.0079
					.33	1.47	.0015

Table 5 (Continued)

Run	Cell Size ($m \times 10^3$)	Phase Volume ($m^3 \times 10^3$)	Agitator Diameter ($m \times 10^3$)	Quinone Concentration ($kg\text{-}mole/m^3$)	Agitator Speed (rps)	Diffusion Current ($A \times 10^3$)	Mass Transfer Coefficient ($m/sec \times 10^3$)
					.67	2.10	.0021
					1.00	2.67	.0027
					1.33	4.35	.0044
					1.70	6.66	.0067
					.33	1.36	.0014
					.33	1.56	.0016
41	102.0	0.7	89.0	0.0005	.33	2.00	.0020
					.70	4.21	.0042
					1.00	8.63	.0086
					.33	1.95	.0020
					.68	3.70	.0037
					1.00	7.50	.0075
					1.37	9.76	.0098
					.33	1.75	.0018
					.33	1.79	.0018
					.70	3.16	.0032
42	102.0	0.9	89.0	0.0005	.33	1.68	.0017
					.67	3.16	.0032
					1.00	6.72	.0068
					1.37	9.14	.0092
					.33	1.48	.0015
					1.00	6.72	.0068
43	102.0	0.9	64.0	0.0005	.33	1.37	.0014
					.67	1.79	.0018
					1.00	2.32	.0023
					1.33	3.05	.0031
					1.73	5.32	.0053
					2.07	7.53	.0076
					.33	1.58	.0016
					1.00	2.32	.0023

Table 5 (Continued)

Run	Cell Size ($m \times 10^3$)	Phase Volume ($m^3 \times 10^3$)	Agitator Diameter ($m \times 10^3$)	Quinone Concentration (kg-mole/m^3)	Agitator Speed (rps)	Diffusion Current ($A \times 10^3$)	Mass Transfer Coefficient (m/sec $\times 10^3$)
46	102.0	0.9	38.0	0.0005	.33	1.01	.0010
					.33	0.70	.0007
					.70	1.18	.0012
					1.03	1.31	.0013
					1.37	1.53	.0015
					1.73	1.67	.0017
					2.00	1.88	.0019
					3.00	2.72	.0027
					3.00	3.17	.0032
					3.67	4.07	.0041
					.33	1.07	.0011
					1.00	1.49	.0015
56	203.0	3.0	190.0	0.0005	.33	12.1	.0030
					.67	40.3	.0101
					.33	10.2	.0026
					.67	36.5	.0092
					1.00	12.4	.0312
					.50	18.1	.0046
					.83	62.5	.0157
					.33	10.2	.0026
57	203.0	3.0	140.0	0.0005	.33	6.00	.0015
					.67	10.0	.0025
					1.00	35.0	.0088
					1.37	83.0	.0209
					.33	5.04	.0013
60	203.0	3.0	89.0	0.0005	.33	3.55	.0009
					.68	5.52	.0014
					1.03	6.89	.0017
					1.40	8.27	.0021
					1.73	11.2	.0028
					2.00	14.8	.0037
					.33	3.15	.0008

Table 5 (Continued)

Run	Cell Size ($m \times 10^3$)	Phase Volume ($m^3 \times 10^3$)	Agitator Diameter ($m \times 10^3$)	Quinone Concentration (kg-mole/m^3)	Agitator Speed (rps)	Diffusion Current ($A \times 10^3$)	Mass Transfer Coefficient (m/sec $\times 10^3$)
66	203.0	7.0	190.0	0.0005	.33	12.1	.0030
					.67	46.4	.0117
					1.00	78.6	.0198
					1.32	161.3	.0406
					.33	10.1	.0025
67	203.0	7.0	140.0	0.0005	.33	5.52	.0014
					.67	10.5	.0027
					1.00	31.1	.0078
					1.33	59.2	.0149
					1.67	113.4	.0285
					.33	5.02	.0013
70	203.0	7.0	89.0	0.0005	.33	3.56	.0009
					.67	4.15	.0010
					1.00	5.24	.0013
					1.33	7.12	.0018
					1.70	12.1	.0030
					1.67	11.6	.0029
					2.07	18.9	.0048
					.33	3.16	.0080
76	305.0	9.0	280.0	0.0002	.33	20.1	.0056
					.53	36.1	.0101
					.67	60.2	.0168
					.82	72.3	.0201
					1.00	120.5	.0336
					.33	15.1	.0042
77	305.0	9.0	240.0	0.0002	.33	6.02	.0017
					.65	30.1	.0084
					1.03	74.3	.0207

Table 5 (Continued)

Run	Cell Size ($m \times 10^3$)	Phase Volume ($m^3 \times 10^3$)	Agitator Diameter ($m \times 10^3$)	Quinone Concentration ($kg\text{-}mole/m^3$)	Agitator Speed (rps)	Diffusion Current ($A \times 10^3$)	Mass Transfer Coefficient ($m/sec \times 10^3$)
					.67	38.2	.0106
					1.30	126.5	.0352
					.33	7.03	.0020
80	305.0	9.0	190.0	0.0002	.33	3.10	.0009
					.67	11.8	.0033
					1.03	28.3	.0079
					1.37	48.2	.0134
					1.67	70.3	.0196
					.33	2.71	.0008
86	305.0	18.0	280.0	0.0002	.33	20.2	.0056
					.50	42.5	.0118
					.67	89.0	.0248
					.83	108.3	.0302
					1.00	153.8	.0428
					.33	16.2	.0045
87	305.0	18.0	240.0	0.0002	.33	8.57	.0024
					.50	23.2	.0066
					.67	54.4	.0152
					1.00	97.8	.0272
					1.33	155.8	.0434
					.33	13.1	.0037
90	305.0	18.0	190.0	0.0002	.33	4.03	.0011
					.67	24.2	.0067
					1.00	51.4	.0143
					1.33	69.6	.0193
					1.67	93.7	.0261
					.33	5.04	.0014

Table 6. Experimental Conditions and Results Measured with 45 wt % Sucrose in the Aqueous Phase

Run	Cell Size ($m \times 10^3$)	Phase Volume ($m^3 \times 10^3$)	Agitator Diameter ($m \times 10^3$)	Quinone Concentration ($kg\text{-}mole/m^3$)	Agitator Speed (rps)	Diffusion Current ($A \times 10^3$)	Mass Transfer Coefficient ($m/sec \times 10^3$)
47	102.0	0.9	89.0	0.0005	.33	0.79	.0008
					.70	2.18	.0022
					1.03	5.31	.0054
					1.40	12.0	.0121
					.33	0.79	.0008
					1.00	5.16	.0052
48	102.0	0.9	64.0	0.0005	.33	0.63	.0006
					.67	0.79	.0008
					1.00	0.95	.0010
					1.37	1.59	.0016
					1.70	2.64	.0027
					2.07	4.54	.0046
					.33	0.63	.0006
					1.03	0.85	.0009
51	102.0	0.9	38.0	0.0005	.33	0.44	.0004
					.33	0.31	.0003
					.67	0.46	.0005
					1.03	0.50	.0005
					1.40	0.57	.0006
					1.73	0.59	.0006
					2.33	0.66	.0007
					3.67	1.05	.0011
					.33	0.31	.0003
					1.03	0.48	.0005
52	102.0	0.7	89.0	0.0005	.33	0.60	.0006
					.67	1.19	.0012
					1.00	4.17	.0042
					1.37	15.0	.0150
					.33	0.60	.0006
					1.00	4.17	.0042

Table 6 (Continued)

Run	Cell Size ($m \times 10^3$)	Phase Volume ($m^3 \times 10^3$)	Agitator Diameter ($m \times 10^3$)	Quinone Concentration (kg-mole/m^3)	Agitator Speed (rps)	Diffusion Current ($A \times 10^3$)	Mass Transfer Coefficient (m/sec $\times 10^3$)
53	102.0	0.7	64.0	0.0005	.33	0.57	.0006
					.33	0.44	.0004
					.70	0.86	.0009
					1.03	1.19	.0012
					1.37	2.08	.0021
					1.77	3.89	.0039
					1.77	3.54	.0036
					2.03	5.36	.0054
					.33	0.49	.0005
					1.00	1.15	.0012
54	102.0	0.7	38.0	0.0005	.33	0.36	.0004
					.33	0.28	.0003
					.67	0.38	.0004
					1.00	0.44	.0004
					1.37	0.53	.0005
					1.73	0.61	.0006
					2.33	0.81	.0008
					3.00	1.06	.0011
					3.67	1.46	.0015
					.33	0.30	.0003
					1.00	0.44	.0004
55	102.0	0.9	38.0	0.0005	.33	0.40	.0004
					.67	0.42	.0004
					1.00	0.50	.0005
					1.33	0.55	.0006
					1.77	0.63	.0006
					2.33	0.85	.0009
					3.67	1.52	.0015
					.33	0.32	.0003
					1.03	0.50	.0005

Table 6 (Continued)

Run	Cell Size ($m \times 10^3$)	Phase Volume ($m^3 \times 10^3$)	Agitator Diameter ($m \times 10^3$)	Quinone Concentration (kg-mole/m^3)	Agitator Speed (rps)	Diffusion Current ($A \times 10^3$)	Mass Transfer Coefficient (m/sec $\times 10^3$)
61	203.0	3.0	190.0	0.0005	.33	4.05	.0010
					.67	23.3	.0059
					1.00	70.0	.0178
					.52	12.1	.0031
					.83	46.6	.0117
					.33	4.05	.0010
62	203.0	3.0	140.0	0.0005	.33	3.01	.0008
					.67	5.52	.0014
					1.00	27.1	.0068
					1.33	51.2	.0129
					.33	3.01	.0008
65	203.0	3.0	89.0	0.0005	.33	1.88	.0005
					.67	2.47	.0006
					1.00	3.26	.0008
					1.33	4.35	.0011
					1.70	5.93	.0015
					2.00	9.00	.0023
					.33	1.78	.0004
71	203.0	7.0	190.0	0.0005	.33	6.10	.0015
					.67	22.4	.0056
					1.00	40.6	.0102
					1.33	76.2	.0192
					0.33	5.08	.0013
72	203.0	7.0	140.0	0.0005	.33	2.02	.0005
					.67	5.04	.0013
					1.00	15.1	.0038
					1.33	32.3	.0081
					1.67	51.9	.0131
					2.00	72.6	.0183
					.33	2.02	.0005

Table 6 (Continued)

Run	Cell Size ($m \times 10^3$)	Phase Volume ($m^3 \times 10^3$)	Agitator Diameter ($m \times 10^3$)	Quinone Concentration (kg-mole/m^3)	Agitator Speed (rps)	Diffusion Current ($A \times 10^3$)	Mass Transfer Coefficient (m/sec $\times 10^3$)
75	203.0	7.0	89.0	0.0005	.33	1.19	.0003
					.67	1.58	.0004
					1.00	2.37	.0006
					1.33	4.74	.0012
					1.67	7.75	.0020
					2.00	17.3	.0043
					2.40	30.2	.0076
					.33	1.19	.0003
81	305.0	9.0	280.0	0.0002	.33	10.2	.0028
					.67	42.8	.0119
					.97	81.6	.0227
					.50	30.6	.0085
					.83	63.2	.0176
					.33	10.2	.0028
82	305.0	9.0	240.0	0.0002	.33	5.04	.0014
					.68	32.3	.0090
					1.00	49.4	.0138
					1.30	94.7	.0264
					.33	8.06	.0023
85	305.0	9.0	190.0	0.0002	.33	1.76	.0005
					.65	9.77	.0027
					.98	23.4	.0065
					1.33	32.8	.0091
					1.67	57.5	.0160
					.33	1.37	.0004
91	305.0	18.0	280.0	0.0002	.33	12.2	.0034
					.53	34.5	.0096
					.70	51.8	.0144
					.87	71.1	.0198
					1.00	87.4	.0243
					.33	8.13	.0023

Table 6 (Continued)

Run	Cell Size ($m \times 10^3$)	Phase Volume ($m^3 \times 10^3$)	Agitator Diameter ($m \times 10^3$)	Quinone Concentration ($kg\text{-}mole/m^3$)	Agitator Speed (rps)	Diffusion Current ($A \times 10^3$)	Mass Transfer Coefficient ($m/sec \times 10^3$)
92	305.0	18.0	240.0	0.0002	.33	5.04	.0014
					.67	36.3	.0101
					1.00	62.5	.0174
					1.33	98.8	.0275
					.33	8.06	.0023
95	305.0	18.0	190.0	0.0002	.33	3.59	.0010
					.67	11.1	.0031
					1.00	32.8	.0091
					1.33	49.4	.0138
					1.67	63.5	.0177
					.33	3.59	.0010

APPENDIX B

MEASUREMENT OF QUINONE DIFFUSION COEFFICIENT

As described in Chapter IV, the diffusion coefficient of quinone through the aqueous electrolyte medium was measured as a function of aqueous viscosity, using the d.m.e. Table 7 lists the experimental conditions and results which, when substituted into Equation (17), can be used to calculate the diffusion coefficient.

Table 7 also gives the sucrose concentration, measured diffusion current, quinone concentration, mercury flow rate, and mercury drop time for each of the measurements. The calculated diffusion coefficients are included in Table 2 (see page 51).

Table 7. Data and Conditions for Quinone Diffusion Coefficient Measurements

Sucrose Concentration (wt %)	Diffusion Current (mA)	Quinone Concentration (millimoles/liter)	Mercury Flow Rate (mg/sec)	Drop Time (sec)
0.0	3.04	1.0	1.001	0.5
34.0	1.19	1.0	1.001	0.5
45.0	0.755	1.0	1.001	0.5

APPENDIX C

SAMPLE CALCULATIONS FOR A TYPICAL MASS TRANSFER RUN

The mass transfer coefficients given in Tables 4, 5, and 6 were calculated from Equation (15), which is:

$$k = \frac{I}{(Z)(F)(A)(C_B)} .$$

The diffusion current is determined from the current-voltage curve for each run (see Figure 3, page 17). The interfacial area available for mass transfer was assumed to be the cross-sectional area of the cell. The quinone concentration was calculated from the amount of quinone used to prepare the electrolyte solution. The quinone concentration was occasionally verified with the d.m.e. apparatus. The calculated mass transfer coefficient for Run 8, which was made at an agitator speed of 0.53 rps, is:

$$k = \frac{62.9 \times 10^{-3} \text{ A}}{(2 \frac{\text{equiv}}{\text{mole}})(96{,}487 \frac{\text{coul}}{\text{equiv}})(1 \frac{\text{A-sec}}{\text{coul}})(0.0412 \text{ m}^2)(1.0 \frac{\text{mole}}{\text{m}^3})}$$

$$= 7.9 \times 10^{-6} \text{ m/sec.}$$

THIS PAGE

WAS INTENTIONALLY

LEFT BLANK

ORNL/TM-6670

INTERNAL DISTRIBUTION

1. J. M. Begovich
2-6. C. H. Brown, Jr.
7. S. D. Clinton
8. R. M. Counce
9. T. M. Gilliam
10. G. L. Haag
11. J. D. Hewitt
12-16. J. R. Hightower, Jr.
17. L. E. McNeese
18. J. P. Meyer
19. J. J. Perona
20. W. W. Pitt
21. B. R. Rodgers
22. C. D. Scott
23. M. G. Stewart
24. J. B. Talbot
25. J. S. Watson
26. M. E. Whatley
27. E. L. Youngblood
28. L. E. Swabb, Jr. (consultant)
29-30. Laboratory Records
31. Laboratory Records, RC
32-33. Central Research Library
34. Document Reference Section
35. ORNL Patent Office

EXTERNAL DISTRIBUTION

36. W. J. Haubach, Office of Basic Energy Sciences, DOE, Washington, D. C. 20545.
37. E. S. Pierce, Office of Basic Energy Sciences, DOE, Washington, D. C. 20545.
38. F. Dee Stevenson, Office of Basic Energy Sciences, DOE Washington, D. C. 20545.
39. Office of Assistant Manager, Energy Research and Development, DOE-ORO, P.O. Box E, Oak Ridge, Tenn. 37830.
40-66. Technical Information Center, Oak Ridge, Tenn. 37830.